Westinghouse Non-Proprietary Class 3

WCAP-14342-A
CENPD-404-NP-A Addendum 1

February 2003

Addendum 1 to WCAP-14342-A And CENPD-404-NP-A Optimized ZIRLO™

Westinghouse Non-Proprietary Class 3

WCAP-14342-A
and CENPD-404-NP-A Addendum 1

Addendum 1 to WCAP-14342-A And CENPD-404-NP-A Optimized ZIRLO™

February 2003

Prepared by

H. H. Shah

Approvals

D. Rowland, Manager
Fuel Licensing
Nuclear Fuel

S. Ray, Manager
Product Engineering
Nuclear Fuel

Copyright Notice

The reports transmitted herewith each bear a Westinghouse copyright notice. The NRC is permitted to make the number of copies of the information contained in these reports which are necessary for its internal use in connection with generic and plant-specific reviews and approvals as well as the issuance, denial, amendment, transfer, renewal, modification, suspension, revocation, or violation of a license, permit, order, or regulation subject to the requirements of 10 CFR 2.790 regarding restrictions on public disclosure to the extent such information has been identified as proprietary by Westinghouse, copyright protection notwithstanding. With respect to the non-proprietary versions of these reports, the NRC is permitted to make the number of copies beyond those necessary for its internal use which are necessary in order to have one copy available for public viewing in the appropriate docket files in the public document room in Washington, DC and in local public document rooms as may be required by NRC regulations if the number of copies submitted is insufficient for this purpose. Copies made by the NRC must include the copyright notice in all instances and the prprietary notice if the original was identified as proprietary.

Table of Contents

Table of Contents for Appendix A: Test Methods

Table of Contents for Appendix B: Test Results

List of Tables

List of Tables for Appendix B: Test Results

List of Figures

List of Figures for Appendix B: Test Results

List of Figures for Appendix B: Test Results

1.0 Introduction

1.1 Purpose

The purpose of this Addendum is to obtain Nuclear Regulatory Commission ("NRC") approval of an extension to the regulatory definition of ZIRLO™ as approved in WCAP-12610-P-A and CENPD-404-P-A. This extension of the regulatory definition of ZIRLO™ is designed to extend the "allowed material composition" to encompass the full range of ZIRLO™ as defined by Westinghouse Electric Company ("Westinghouse") and as described in this topical report. The proposed change allows for the optimization of ZIRLO™ for enhanced corrosion resistance.

The optimization of the material composition of the current licensed material ZIRLO™ to Optimized ZIRLO™ is similar to the approach used to extend the material composition of Zircaloy-4 to "Improved Zircaloy-4" (i.e., a slight reduction in tin content for improved in-reactor corrosion resistance). As in the case of Zircaloy-4 and as demonstrated by this report, a minor material composition change does not appreciably change the ZIRLO™ physical or mechanical properties or have any appreciable impact on analysis models and methods. This change is designed to enhance corrosion resistance of the ZIRLO™ material in more adverse in-reactor primary chemistry environments and at higher fuel duties with higher burnups.

This Addendum provides details and results of material testing of the Optimized ZIRLO™ (hereafter referred to as "Optimized ZIRLO™") compared to the current licensed ZIRLO™ (hereafter referred to as "Standard ZIRLO™") and demonstrates that the Standard ZIRLO™ material properties utilized in various models and methodologies can be applied to analyses of Optimized ZIRLO™.

1.2 ZIRLO™ Definition

ZIRLO™ material was first licensed by the NRC as part of the VANTAGE+ fuel product in WCAP-12610 (Reference 1). The topical report received NRC (Reference 2) approval in July 1991 and the approved version (Reference 3) was issued with all the associated NRC Safety Evaluations (SE) for the base document and the various appendices in April 1995. In August 1992, the NRC promulgated a regulatory change (Reference 4) to 10 CFR 50.44, 10 CFR 50.46, and 10 CFR Part 50 Appendix K to allow the use of ZIRLO™ without obtaining exemption approval. Between July 1991 and August 1992, Westinghouse had numerous meetings with the NRC, and in particular, the Office of the General Counsel (OGC), to describe ZIRLO™ and to obtain a change in the Code of Federal Regulations (CFRs). Based

on information presented to the NRC during this period, the description of ZIRLO™ material in both the NRC SE and Appendix A of WCAP-12610, and also accounting for descriptions of ZIRLO™ in patent documents, the following definition is the basis for the ZIRLO™ material licensed by the NRC in both WCAP-12610 and in changing the Code of Federal Regulations.

> "ZIRLO™ alloy is Westinghouse's 1% niobium-tin-iron zirconium-based alloy having a microstructure comprising second phase precipitates (specifically, a body-centered cubic beta-niobium-zirconium phase and a hexagonal zirconium-niobium-iron inter-metallic phase) homogeneously distributed throughout the zirconium matrix. ZIRLO™ is a modification of Zircaloy-4 that includes a reduction in the tin, iron and chromium content, and addition of nominally one percent niobium."

Based on the above definition of ZIRLO™, the numerous meetings held between Westinghouse and the NRC; the technical justification of ZIRLO™ as documented in WCAP-12610 (Reference 3); and the technical review of ZIRLO™ as documented in Reference 2, the changes to 10 CFR 50.44, 10 CFR 50.46, and 10 CFR Part 50 Appendix K were made and noticed to the public in Reference 4. The proposed optimization of ZIRLO™ still meets the above definition of ZIRLO™. This Addendum provides the technical justification that the optimization of ZIRLO™ does not invalidate any of the bases for ZIRLO™ that the NRC previously reviewed and approved. Thus the optimization of the ZIRLO™ material will only result in a slight change in the material composition of ZIRLO™ and the material will still be ZIRLO™, similar to the optimization of Zircaloy-4.

1.3 Applicability (WCAP-12610-P-A & CENPD-404-P-A)

Both WCAP-12610-P-A (Reference 3) and CENPD-404-P-A (Reference 5) define the material properties for licensed ZIRLO™. This Addendum covers both topicals and demonstrates that Standard ZIRLO™ material properties currently utilized in various models and methodologies are applicable to analyses of Optimized ZIRLO™.

2.0 Material Specification

2.1 Original Licensing Basis

As noted in the previous section, the material composition of ZIRLO™ is specified in Appendix A of WCAP-12610-P-A. Specifically, the wording in Appendix A is as follows:

> "ZIRLO™ represents a modification of Zircaloy-4 which has been achieved by reducing the tin and iron content, eliminating the chromium content, and adding one percent niobium. The following table compares the two alloys:

Element	ZIRLO™ Alloy	Zircaloy-4 Alloy
Sn, wt %	0.8 – 1.2	1.2 – 1.7
Fe, wt %	0.09 – 0.13	0.18 – 0.24
Cr, wt %	--	0.07 – 0.13
Fe + Cr, wt %	--	0.28 – 0.37
Nb, wt %	0.8 – 1.2	--
Zr, wt %	Balance	Balance"

2.2 Revised Licensing Basis

As noted in Section 1.1, this Addendum defines the optimized material composition of ZIRLO™ (or "Optimized ZIRLO™") and demonstrates that the material is essentially the same as the currently licensed ZIRLO™. Optimized ZIRLO™ meets the definition of ZIRLO™ provided to the NRC during the period when the regulatory change was obtained to the Code of Federal Regulations. Therefore, the proposed change to the above wording is as follows:

> "ZIRLO™ alloy is Westinghouse's 1% niobium-tin-iron zirconium-based alloy having a microstructure comprised of second phase precipitates (specifically, a body-centered cubic beta-niobium-zirconium phase and a hexagonal zirconium-niobium-iron inter-metallic phase) homogeneously distributed throughout the zirconium matrix. ZIRLO™ is a modification of Zircaloy-4 that includes a reduction in the tin, iron and chromium content, and addition of nominally one percent niobium. The following table compares the two alloys:

Element	ZIRLO™ Alloy	Zircaloy-4 Alloy
Sn, wt %	0.6 – 1.2	1.2 – 1.7
Fe, wt %	0.09 – 0.13	0.18 – 0.24
Cr, wt %	--	0.07 – 0.13
Fe + Cr, wt %	--	0.28 – 0.37
Nb, wt %	0.8 – 1.2	--
Zr, wt %	Balance	Balance"

The remainder of this Addendum documents material properties for Standard ZIRLO™ material versus the Optimized ZIRLO™ material and shows the differences to be negligible and that any minor differences have no appreciable impact on any design or safety analysis area.

3.0 Material Properties and ZIRLO™ Testing

3.1 Tin Content - Lower Bound Limit

[ ] [a, c] of Optimized ZIRLO™ were sectioned from different and randomly selected tubes and sent to the Westinghouse Western Zirconium Plant for detailed chemical analyses using standard production equipment and procedures. Samples from each of the [ ] [a, c]. A summary of the tin content is shown in the table below.

Table 3.1-1
Nominal Measured Tin Content

[ ] a, b, c

Based on a statistical analysis, the tin content range is as follows:

[ ] a, b, c

Based on the above review, it can be seen that the test material used for the analysis has a tin content in the range of [ ] [a, b, c], which supports a lower bound limit of 0.6%.

It should be noted that "[ ] [a, c]" tin content referred to in various tables and text throughout this document refers to a nominal tin content. Actual tin content of the lots used for testing is as stated above.

3.2 ZIRLO™ Test Program

A series of tests of key characteristics for both Standard ZIRLO™ material and the Optimized ZIRLO™ have been performed (refer to Table 3.3-1). The test data have been evaluated by various disciplines to determine the relative impact of the change to Optimized ZIRLO™ and to show that the Optimized ZIRLO™ is essentially the same as Standard ZIRLO™.

The currently licensed minimum tin content of ZIRLO™ is 0.8%. The proposed revision of minimum tin content is 0.6%. No other changes in ZIRLO™ composition are proposed. Therefore, there is only a minimal impact on the associated models and methods, which have been confirmed by the various tests and evaluations conducted and documented in this report.

3.3 Properties Tested

The physical, mechanical, microstructural and LOCA related testing of the Optimized ZIRLO™ material is delineated in the table below (Table 3.3-1). Test procedures and results are specified in Appendices A and B, respectively.

Table 3.3-1
Summary of Tests Conducted

a, c

3.4 Test Facilities

Thermophysical Properties Research Laboratory, Inc. (TPRL), 3080 Kent Avenue, West Lafayette, IN 47906. Contact: [ ]^{a,c}. Thermophysical properties were measured at TPRL under the observation of Westinghouse personnel according to TPRL procedures. NIST traceable calibration standards were used during the course of testing performed at TPRL. The results were formally reported to Westinghouse.

UJP-Praha (formerly SKODA-UJP), Nad Kaminkou 1345, 156 10 Praha 5 - Zbraslav, Czech Republic. Contact: [ ]^{a,c}. UJP-Praha is a ISO 9001 certified facility. Oxidation weight gain measurements were performed according to ASTM G2M-88 specifications and formally reported to Westinghouse.

Commissariat a l'Énergie Atomique – Centre De Saclay (CEA-Saclay), 91191 Gif Sur Yvette Cedex, France. Contact: [ ]^{a,c}. CEA-Saclay is a French national laboratory and ISO-9001 certified facility. The Department of Nuclear Materials performed high temperature creep tests using the EDGAR-2 facility and methodologies to evaluate the high temperature creep performance of ZIRLO™. The results were formally provided to Westinghouse.

Tests were also performed at various Westinghouse sites: Science and Technology Department, George Westinghouse Research & Technology Park, 1340 Beulah Road, Churchill, PA 15235; Western Zirconium Plant, Nuclear Fuel, 10,000 W. 900 S., Ogden, Utah 84404-9799; and the Columbia Site, Nuclear Fuel, 5801 Bluff Road, Columbia, SC 29250. All Westinghouse test facilities are governed by the Westinghouse Quality Management System (QMS). The Westinghouse QMS system is frequently reviewed by the NRC to ensure compliance with the Code of Federal Regulations. Revision 5 of the Westinghouse QMS received NRC approval in a letter from the NRC to Westinghouse, dated September 13, 2002. Westinghouse is also ASME and ISO-9001 certified.

3.5 Irradiation Experience

The Optimized ZIRLO™ material has been used in Lead Test Assemblies (LTAs) in several plants, domestically and internationally. A list of those plants where Optimized ZIRLO™ has been tested is summarized below:

[a, c]

The following three figures provide representative in-reactor performance results for the Optimized ZIRLO™.

Figure 3.5-1
Irradiation Experience – Rod Oxide

[a, b , c]

Figure 3.5-2
Irradiation Experience – Rod Growth

a, b, c

Figure 3.5-3
Irradiation Experience – Assembly Growth

a, b, c

4.0 Fuel Design and Accident Analysis Effects

4.1 Fuel Assembly Mechanical Design

The fuel assembly designs can be impacted by [

] [a, c] however the mechanical strength of the [

] [a, b, c] The minimum yield strength value for Optimized ZIRLO™ is [ ] [a, c]

Similar relationship exists for other material conditions. Thus, the Optimized ZIRLO™ will meet the existing fuel assembly material design criteria. The other area of fuel assembly design that is affected by the change from Standard ZIRLO™ to Optimized ZIRLO™ is the reduction in corrosion or oxidation and a corresponding reduction in hydrogen pickup. These later impacts are benefits with respect to the final assembly structural capability and with respect to fuel assembly growth considerations.

The other key area of the fuel assembly design that must be addressed, when considering the [

] [a, c]. The grid assembly must withstand the dynamic loads from Condition I and II events, including Operating Basis Earthquake (OBE). Grid deformation due to the most limiting dynamic loads resulting from Condition III and IV events, including Safe Shutdown Earthquake (SSE) and Loss-of-Coolant-Accident (LOCA), must not result in unacceptable guide thimble tube distortion, which could impede control rod insertion. The flow channel area reduction must not cause the peak cladding temperature to exceed 2200 °F during a LOCA event.

Therefore, grid impact testing was performed, at operating temperature (600 °F) in air, to determine the impact crush strength and stiffness of the Standard ZIRLO™ and Optimized ZIRLO™ for a representative Westinghouse mid-grid. The table below details the results and shows that the [

] [a, c].

[a, b, c]

Based on the [ ] [a, c] for the Optimized ZIRLO™, the satisfaction of the SSE/LOCA design criteria for the ZIRLO™ mid-grid design will not be affected by the use of Optimized ZIRLO™ for the grid assemblies.

4.2 Fuel Rod Design

Since Westinghouse has two fuel performance codes (PAD 4.0 and FATES3B) and two fuel rod design methodologies (Westinghouse fuel designs and CE fuel designs), the change to Optimized ZIRLO™ from Standard ZIRLO™, with respect to these codes and methods, will be addressed separately.

4.2.1 Westinghouse Fuel Design

The Westinghouse fuel designs are analyzed to the following design criteria[3]. Each criterion is specified along with the evaluation of the use of Optimized ZIRLO™ on the specific criterion.

- Rod Internal Pressure - Gap Reopening Limit/DNB Propagation

  Criterion: The internal pressure of the lead fuel rod in the reactor will be limited to a value below that which could cause the diametrical gap to increase due to outward cladding creep during steady state operation and the internal pressure of the lead fuel rod in the reactor will be limited to a value below that which could cause extensive DNB propagation to occur.

  Evaluation: There is no effect of Optimized ZIRLO™ on the [ ]* [a, c] thus, there will be no effect on evaluating the gap reopening limit criterion. Since there is no effect of Optimized ZIRLO™ on the rod internal pressure, there will be no effect on evaluating the DNB propagation.

- Clad Stress

  Criterion: The design limit for the fuel rod clad stress is that the volume average effective stress calculated with the von Mises equation considering interference due to uniform cylindrical pellet-cladding contact, caused by pellet thermal expansion, pellet swelling and uniform cladding creep, and pressure differences, is less than the ZIRLO™ 0.2% offset yield stress under Condition I and II modes of operation, with due consideration to temperature and irradiation effects. While the cladding has some capability for accommodating plastic strain, the yield stress has been established as the conservative design limit.

---

[*] [a, c]

Evaluation: There is no effect of Optimized ZIRLO™ on the [ ] * [a, c] Therefore, there will be no effect on evaluating the clad stress.

- Clad Strain - Steady State/Transient

Criterion: The design limit for the fuel rod clad strain is the total plastic tensile creep strain due to uniform cladding creep and uniform cylindrical fuel pellet expansion due to swelling and thermal expansion is less than 1% from the unirradiated condition, and that the total tensile strain due to uniform cylindrical pellet thermal expansion during a transient is less than 1% from the pre-transient value.

Evaluation: There is no effect of Optimized ZIRLO™ on the [ ] *[a, c]. Therefore, there will be no effect on evaluating the transient clad strain.

- Corrosion

Criterion: The corrosion-related licensing criteria for the fuel rod cladding are:

1. The ZIRLO™ cladding metal-oxide interface temperature shall not exceed the following limits:
   Steady-State Operation [ ] [a, b, c]
   Condition II Transients [ ] [a, b, c]
2. The best estimate hydrogen pickup in the ZIRLO™ cladding shall not exceed [ ] [a, c] at end of life.
3. The steady-state ZIRLO™ cladding oxidation must be considered in the calculation of the total local oxidation in the Loss of Coolant Accident (LOCA). The 10 CFR 50.46 acceptance criterion is that the maximum total localized oxidation shall not exceed 17% of the cladding thickness.

Evaluation: Optimized ZIRLO™ will be modeled with approved ZIRLO™ corrosion model. Therefore, there will be no impact on evaluating the clad corrosion criterion.

- Fuel Temperatures

Criterion: For Condition I and II events, the fuel system and protection system are designed to assure that a calculated centerline fuel temperature does not exceed the fuel melting temperature. The melting temperature of UO_2 is taken to be 5080 °F (unirradiated) and to decrease 58 °F per 10,000 MWD/MTU fuel burnup.

Evaluation: There is no change in the [ ] [a, b, c]. Therefore, there will be no effect of Optimized ZIRLO™ on the fuel temperature criterion evaluation.

---

[*] [a, c]
[*] [a, c]

- Clad Free Standing

  Criterion: The cladding shall be short-term free standing at beginning of life, at power, and during hot hydrostatic testing.

  Evaluation: The criterion is bounded by generic fuel assembly design analyses such as documented in References 3, 6 and 7. The assumptions made in the generic analyses are not affected by Optimized ZIRLO™.

- Clad Fatigue

  Criterion: The fatigue life usage factor is limited to less than 1.0 to prevent reaching the material fatigue limit.

  Evaluation: There is no change in the [ ]^{a,c}. Therefore, there will be no effect of Optimized ZIRLO™ on the clad fatigue evaluation.

- Plenum Clad Support

  Criterion: The fuel rod in the unsupported plenum region will not collapse during normal operating conditions, nor distort so as to degrade fuel rod performance or preclude rod reconstitution during the assembly design lifetime.

  Evaluation: There is no change to the [ ]^{a,c}. Therefore, there will be no effect of Optimized ZIRLO™ on the plenum clad support evaluation.

- Clad Flattening

  Criterion: The fuel rod design shall preclude clad flattening during the projected exposure.

  Evaluation: There is no change to the [ ]^{a,c}. Therefore, there will be no effect of Optimized ZIRLO™ on the clad flattening analysis.

- Rod Growth

  Criterion: The fuel rods will be designed with adequate clearance between the fuel rod and the top and bottom nozzles to accommodate the differences in the growth of fuel rods and the growth of the fuel assembly.

  Evaluation: There is no change to the [ ]^{a,c}. Therefore, there will be no effect of Optimized ZIRLO™ on the rod growth evaluation.

- Fuel Rod End-Plug Weld Integrity

  Criterion: The fuel rod end plug shall maintain its integrity during Condition I and II events and shall not contribute to any additional fuel failures above those already considered for Condition III and IV events.

  Evaluation: There is no change in the [ ]^{a,c}. Therefore, there will be no effect of Optimized ZIRLO™ on the fuel rod end plug weld integrity evaluation.

4.2.2 CE Fuel Design

The CE fuel designs are analyzed to the following design criteria (Reference 5). Each criterion is specified along with the results of an evaluation of the continued use of Standard ZIRLO™ properties and models for Optimized ZIRLO™ in the analyses performed with the Standard ZIRLO™ properties and models to satisfy each specific criterion

- Maximum Internal Gas Pressure

  Criterion: The fuel rod internal hot gas pressure shall not exceed the critical maximum pressure determined to cause an outward clad creep rate that is in excess of the fuel radial growth rate anywhere locally along the entire active fuel length of the fuel rod.

  Evaluation: Maximum internal gas pressure depends on [ ]^{a,c}. The critical pressure limit for NCLO (No Clad Lift-Off) depends on [ ]^{a,c} during normal operation. An evaluation demonstrated that the application of Standard ZIRLO™ properties and models to Optimized ZIRLO™ will have no impact on maximum internal pressure and will have a conservative impact on the NCLO critical pressure limit. Thus, there will be no effect of Optimized ZIRLO™ on the maximum internal pressure criterion evaluation.

- Excessive Fuel Rod DNB Propagation

  Criterion: The radiological dose consequences of DNB failures shall remain within the specified limits.

  Evaluation: Calculation of DNB propagation depends on [ ]^{a,c}. An evaluation demonstrated that application of Standard ZIRLO™ properties and models to Optimized ZIRLO™ will have no impact on [ ]^{a,c} and that the Standard ZIRLO™ [ ]^{a,c} can be applied to Optimized ZIRLO™. Thus, there will be no effect of Optimized ZIRLO™ on the fuel rod DNB propagation criterion evaluation and no change in contribution to dose.

- Fuel Rod Stress

Criterion: (1) During Conditions 1 and 2, the primary tensile stress in the clad and the end cap welds must not exceed 2/3 of the minimum unirradiated yield strength of the material at the applicable temperature. During Condition 3, the primary tensile stress limit is the yield strength and during Condition 4 seismic and LOCA (mechanical excitation only) conditions the stress limit is the lesser of 0.7 Su or 2.4 Sm.

(2) During Conditions 1, 2 and 3, primary compressive stress in the clad and the end cap welds must not exceed the minimum unirradiated yield strength of the material at the applicable temperature. During Condition 4 seismic and LOCA (mechanical excitation only) conditions the stress limit is the lesser of 0.7 Su or 2.4 Sm.

Evaluation: The above fuel rod stress criteria have been evaluated for the most recent 14x14 and 16x16 fuel designs containing Standard ZIRLO™ cladding and found to be satisfied. Those evaluations considered [ ] [a, c]. All of these parameters involve the material properties and capabilities of the cladding. An evaluation demonstrated that the application of Standard ZIRLO™ properties and models for all properties and models, except corrosion, to Optimized ZIRLO™, will have no impact on maximum stress. Application of Standard ZIRLO™ corrosion properties and models to Optimized ZIRLO™ is conservative in terms of calculated maximum stress. However, since the [ ] [a, c] for Optimized ZIRLO™, minor margin reductions are expected for fuel rods with Optimized ZIRLO™ cladding in the maximum stress criterion evaluation when the conservative treatment of corrosion is ignored.

- Fuel Rod Strain

Criterion: (1) At any time during the fuel or integral-burnable-absorber rod lifetime, the net unrecoverable circumferential tensile cladding strain shall not exceed 1% based on Beginning-of-Life (BOL) cladding dimensions. This criterion is applicable to normal operating conditions, and following a single Condition 2 or 3 event or a single Anticipated Operational Occurrence (AOO).

(2) For fuel or integral-burnable-absorber rods having axial average burnups greater than 52 MWD/KGU, the total (elastic + plastic) circumferential cladding strain increment produced as a result of a single Condition 2 or 3 event, or a single AOO, shall not exceed 1%.

Evaluation: The above fuel rod strain criteria have been evaluated for the most recent 14x14 and 16x16 fuel designs containing Standard ZIRLO™ cladding and found to be satisfied. Those evaluations considered [ ] [a, c]. Further, an evaluation demonstrated that the application of Standard ZIRLO™ properties and models to Optimized ZIRLO™ will have no impact on maximum cladding strain. Thus, there will be no effect of Optimized ZIRLO™ on the cladding strain criterion evaluation.

- Maximum Fuel Temperature

  Criterion: The fuel rod centerline temperature shall not exceed the fuel melt temperature, accounting for degradation due to burnup and addition of burnable absorbers.

  Evaluation: An evaluation demonstrated that the application of Standard ZIRLO™ properties and models to Optimized ZIRLO™ will have no impact on maximum fuel temperature. Thus, there will be no effect of Optimized ZIRLO™ on the maximum fuel temperature criterion evaluation.

- Fuel Rod Fatigue Damage

  Criterion: For the number and types of transients which occur during Condition 1 reactor operation, End-of-Life (EOL) cumulative fatigue damage in the clad and in the end cap welds must be less than 0.8.

  Evaluation: The above fuel rod fatigue damage criterion has been evaluated for the most recent 14x14 and 16x16 fuel designs containing Standard ZIRLO™ cladding and found to be satisfied. The evaluations considered [ ] [a, c]. An evaluation demonstrated that the application of Standard ZIRLO™ properties and models to Optimized ZIRLO™ will have no impact on maximum cladding fatigue damage. Thus, there will be no effect of Optimized ZIRLO™ on the cladding fatigue damage criterion evaluation.

- Cladding Creep Collapse

  Criterion: The time required for the radial buckling of the clad in any fuel or integral-burnable-absorber rod must exceed the reactor operating time necessary for the appropriate batch to accumulate its design average discharge burnup. This criterion must be satisfied for continuous reactor operation at any reasonable power level and during any Condition 1, 2 or 3 situation. It will be considered satisfied if it can be demonstrated that axial gaps longer than 0.125 inch will not occur between fuel pellets and the plenum spring radial support capacity is sufficient to prevent clad collapse under all design conditions.

  Evaluation: The above fuel rod clad collapse criterion has been evaluated for the most recent 14x14 and 16x16 fuel designs containing Standard ZIRLO™ cladding and found to be satisfied. Those evaluations considered [ ] [a, c]. An evaluation demonstrated that the application of Standard ZIRLO™ properties and models for all properties and models except corrosion to Optimized ZIRLO™ will have no impact on maximum stress. Application of Standard ZIRLO™ corrosion properties and models to Optimized ZIRLO™ is conservative in terms of calculated creep collapse. Thus, there will be no effect of Optimized ZIRLO™ on the cladding creep collapse criterion evaluation.

- Shoulder Gap

  Criterion: The axial length between end fittings must be sufficient to accommodate differential thermal expansion and irradiation-induced differential growth between fuel rods and guide tubes such that it can be shown with 95% confidence that no interference exists.

  Evaluation: The above design criterion is commonly referred to as shoulder gap and is evaluated using the [ ]^{a,c} of the fuel rod cladding. This criterion has been evaluated for the most recent 14x14 and 16x16 fuel designs containing Standard ZIRLO™ cladding and found to be satisfied. An evaluation demonstrated that the application of Standard ZIRLO™ properties and models to Optimized ZIRLO™ will have no impact on predicted shoulder gap. Thus, there will be no effect of Optimized ZIRLO™ on the shoulder gap criterion evaluation.

- Seismic and LOCA Loads

  Criterion: The fuel rod cladding shall be capable of withstanding the loads resulting from the mechanical excitations occurring during the seismic and/or LOCA without failure resulting from excessive primary stresses.

  Evaluation: The analysis methodology is unaffected by the change to Optimized ZIRLO™. Minor changes to allowable stress margins may occur but there will be no impact since significant stress margins exist for cladding under the postulated loading conditions.

- Corrosion

  Criterion: The predicted best-estimate ZIRLO™. cladding corrosion will remain below 100 microns for all locations on the fuel.

  Evaluation: The Standard ZIRLO™ corrosion model will be used to model Optimized ZIRLO™. Thus, there will be no effect on the clad corrosion criterion evaluation.

4.3 Nuclear Design

As documented in References 3 and 5, the only effect of ZIRLO™ alloy on the nuclear design analytical models and methods is a slight enrichment penalty due to the presence of niobium. This enrichment penalty has a negligible effect on the nuclear analysis, even for full core ZIRLO™ analyses. Since the Optimized ZIRLO™ remains unchanged, with respect to the niobium content, there is no change in the nuclear analysis of a reload core. The ZIRLO™ composition is not explicitly modeled in nuclear design calculations.

4.4 Thermal and Hydraulic Design

As documented in previous topicals, the use of ZIRLO™ cladding or structural materials for the fuel assembly skeleton has no impact on the thermal-hydraulic analysis since the material properties are not modeled. The thermal-hydraulic analysis depends on the fuel assembly geometric conditions, the cladding surface finish and the heat transferred to the surface of the cladding. Since the [

] [a, c] in the Optimized ZIRLO™

will have no effect on the thermal-hydraulic analysis.

4.5 Non-LOCA Accident Design

Section 5.1 of Reference 3 and Section 7.0 of Reference 5 describe the non-LOCA evaluations that were completed to support the introduction of ZIRLO™ cladding for Westinghouse and CE fuel designs, respectively. As discussed therein, the only difference of any consequence between Zircaloy-4 and ZIRLO™ was the change in specific heat, which was modeled in FACTRAN and STRIKIN-II and evaluated for the Locked Rotor/Sheared Shaft and Rod Ejection events. [

] [a, c] These evaluations concluded that the change in specific heat had a negligible effect on results for the Locked Rotor/Sheared Shaft and Rod Ejection events.

As shown in Section B.2, the specific heats of Standard and Optimized ZIRLO™ are approximately equal within the accuracy of the data. Since the differences in specific heat between Zircaloy-4 and ZIRLO™ were previously determined to have either no effect or a negligible effect on non-LOCA transient results, the change from Standard to Optimized ZIRLO™ would also have either no effect or a negligible effect on non-LOCA transient results.

4.6 LOCA Design (Large Break and Small Break)

4.6.1 W ECCS Performance Evaluation Models

This section evaluates the Optimized ZIRLO™ cladding test results with respect to Large Break LOCA (Appendix K, Best Estimate, and SECY) and Small Break LOCA (Appendix K). Any differences between Standard and Optimized ZIRLO™ grids, thimble tubes, and instrument tubes are considered to

have a negligible effect on Large and Small Break LOCA analysis results, so these components are not considered further here.

Specific Heat

Specific heat measurements for Standard and Optimized ZIRLO™ were taken at the Thermophysical Properties Research Laboratory. [

] [a, c] As discussed in Section B.2, the specific heats of Standard and Optimized ZIRLO™ are approximately equal within the accuracy of the data, with differences that are considered negligible for Large and Small Break LOCA.

Figure 4.6.1-1 compares the ZIRLO™ cladding specific heat models used in LOCBART and SBLOCTA ("Appendix K Model") and WCOBRA/TRAC ("Best Estimate Model") to the Standard and Optimized ZIRLO™ "Heating" data from Table B.2-1. (The "Cooling" data from Table B.2-1 are of minimal importance for licensing-basis LOCA transients, and are not considered further here.) Figure 4.6.1-1 indicates some disagreement between the models and the data that has been resolved as follows:

- For Appendix K Large Break LOCA, sensitivity calculations using the LOCBART code indicated that the differences between the model and data could lead to an increase in peak cladding temperature for some transients. To resolve these differences, the ZIRLO™ cladding specific heat model in LOCBART was modified to reflect the new Standard ZIRLO™ data. This change is being reported separately as an evaluation model change pursuant to 10 CFR 50.46, and any further differences in cladding specific heat between Standard and Optimized ZIRLO™ are considered negligible.

- For Appendix K Small Break LOCA, sensitivity calculations using the SBLOCTA code indicated that the differences between the model and data produce a negligible effect on results. However, for consistency with LOCBART, the ZIRLO™ cladding specific heat model in SBLOCTA was modified to reflect the new Standard ZIRLO™ data. This change is being reported separately as an evaluation model change pursuant to 10 CFR 50.46, and any further differences in cladding specific heat between Standard and Optimized ZIRLO™ are considered negligible.

- As shown in Figure 4.6.1-1, the model used in WCOBRA/TRAC for ZIRLO™ cladding specific heat shows better agreement with the data than the Appendix K model. (Note that the Best Estimate and SECY versions of WCOBRA/TRAC use the same model, and that HOTSPOT uses an approximation of the WCOBRA/TRAC model.) The main differences occur for temperatures between 1400 and 1600°F, which affect a relatively minor portion of a limiting large break LOCA transient and are considered negligible. This assessment is supported by sensitivity calculations using HOTSPOT, which showed that the differences between the ZIRLO™ model and the Optimized ZIRLO™ data produced a minimal effect on results. As a result, the ZIRLO™ cladding specific heat models in Best Estimate and SECY Large Break LOCA can reasonably be applied to Optimized ZIRLO™, and need not be modified to reflect the new Standard ZIRLO™ data.

Figure 4.6.1-1
Comparison of Specific Heat Data

a, b, c

[

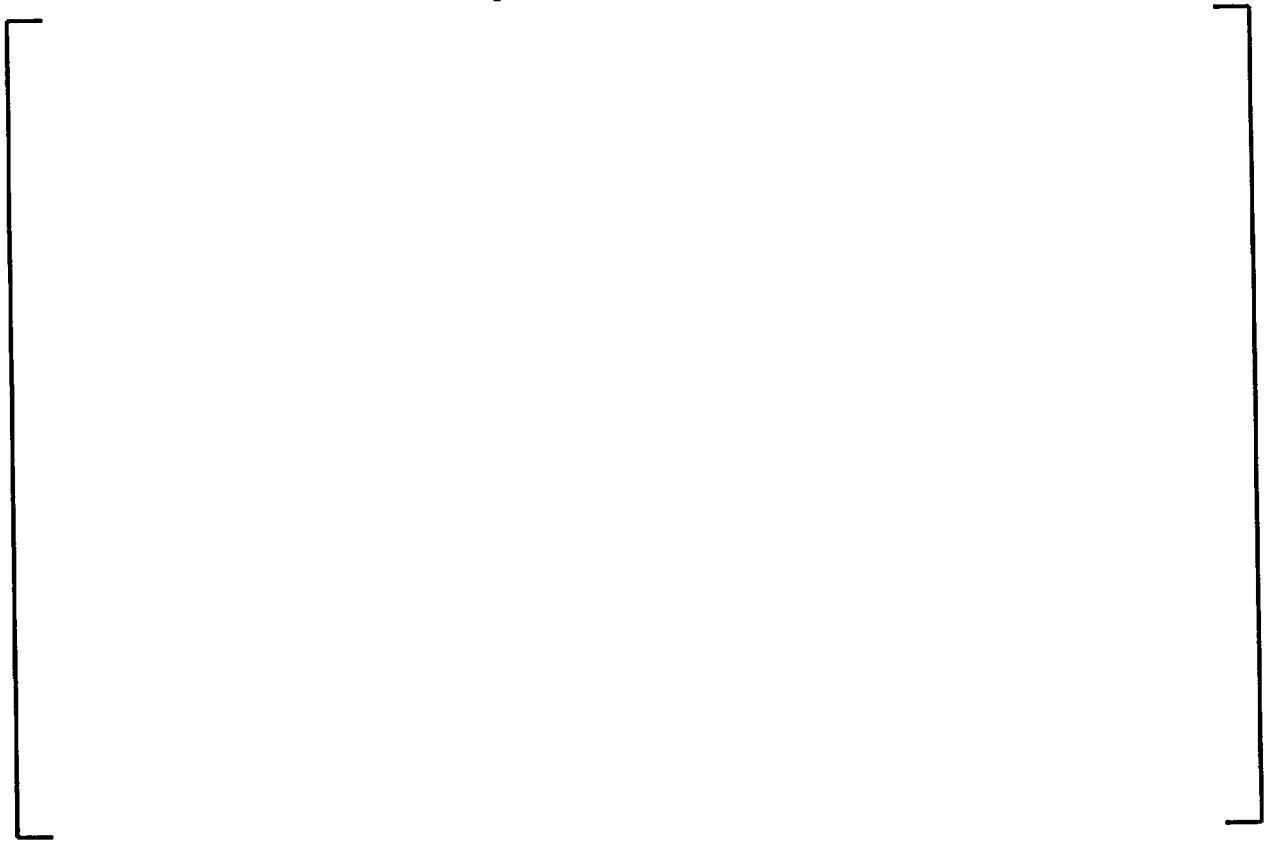

]

Thermal Conductivity

Thermal diffusivity measurements for Standard and Optimized ZIRLO™ were taken at the Thermophysical Properties Research Laboratory. [

] a, b, c As discussed in Section B.3, the thermal conductivities of Standard and Optimized ZIRLO™ are approximately equal within the accuracy of the data, with differences that are considered negligible for Large and Small Break LOCA.

Figure 4.6.1-2 compares the ZIRLO™ cladding thermal conductivity models used in LOCBART and SBLOCTA ("Appendix K Model") and WCOBRA/TRAC ("Best Estimate Model") to the Standard and Optimized ZIRLO™ data from Table B.3-1. For Appendix K Large Break LOCA, sensitivity calculations using the LOCBART code indicated that the differences between the ZIRLO™ model and the Optimized ZIRLO™ data produce a negligible effect on results. This is consistent with the expected result, since radial temperature gradients in the cladding are of minimal importance for typical licensing-basis Large and Small Break LOCA transients. As a result, the ZIRLO™ cladding thermal conductivity model used in LOCBART can reasonably be applied to Optimized ZIRLO™, and need not be modified to reflect the new Standard ZIRLO™ data. These conclusions are also considered to apply to Best Estimate and SECY Large Break LOCA and Appendix K Small Break LOCA, which would be similarly insensitive to reasonable variations in the cladding thermal conductivity.

Figure 4.6.1-2
Comparison of Thermal Conductivity Data

a, b, c

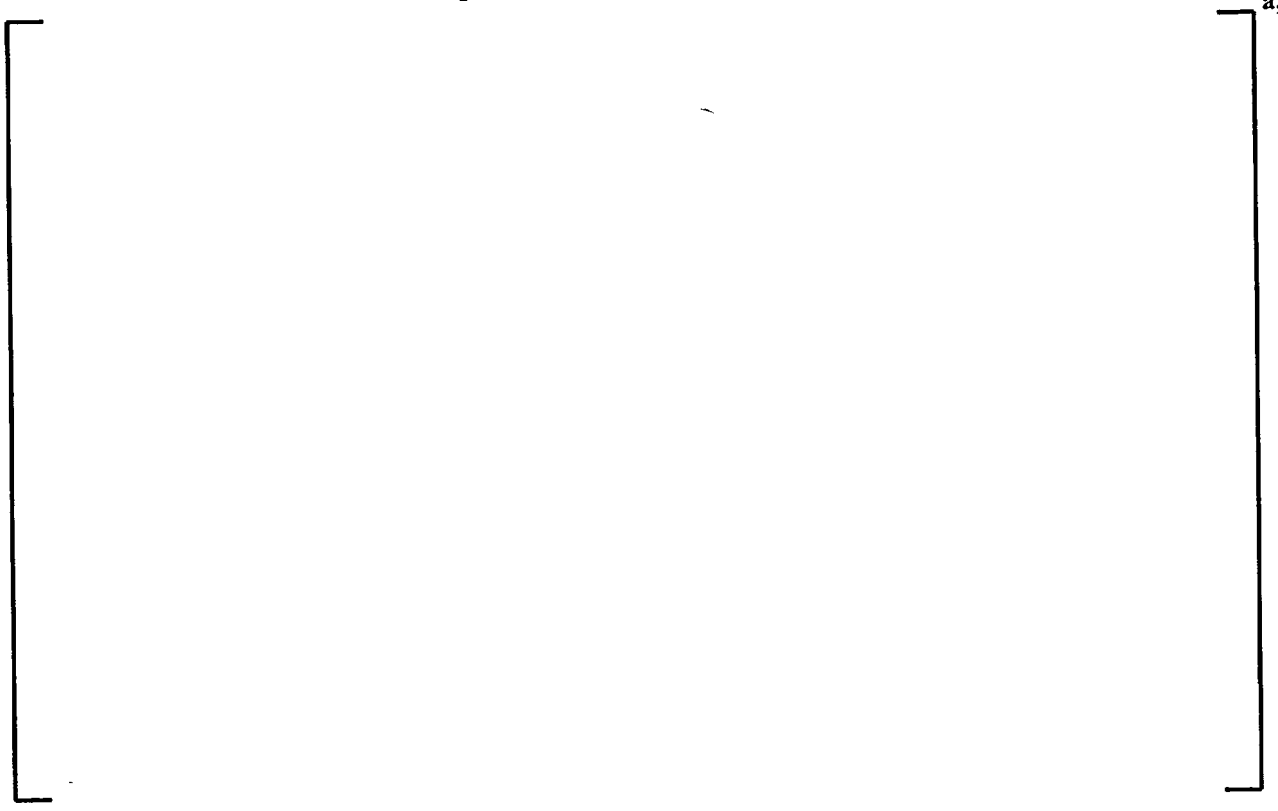

Emissivity

Measurements of the hemispherical total emissivity for Standard and Optimized ZIRLO™ were taken at the Thermophysical Properties Research Laboratory. [

.] [a, c] As shown in Section B.4, the emissivities of Standard and Optimized ZIRLO™ are approximately equal within the accuracy of the data, with differences that are considered negligible for Large and Small Break LOCA.

[

] [a, b, c]

Burst Temperature, Burst Strain, and Assembly Blockage

Measurements of the burst temperature and circumferential burst strain for Standard and Optimized ZIRLO™ cladding were taken at the Columbia Burst Test Facility. [

] [a, c] As discussed in Section B.13, the burst temperature and circumferential burst strain were found to be in reasonable agreement with the prior ZIRLO™ test data from Reference 3.

Review of the pertinent code documentation indicates that the burst and blockage models vary somewhat from code to code, particularly in Best Estimate Large Break LOCA where the stochastic treatment of burst phenomena in HOTSPOT is fundamentally different than the deterministic approach used in other evaluation models. Since the new test data are effectively indistinguishable from the data upon which all of the current ZIRLO™ models are ultimately based, it is concluded that the current ZIRLO™ models for burst temperature and circumferential burst strain (and assembly blockage, which is based on a geometric conversion of the burst strain) can reasonably be applied to Optimized ZIRLO™, and need not be modified to reflect the new Standard ZIRLO™ data.

High-Temperature Creep

High-temperature creep measurements for Standard and Optimized ZIRLO™ were taken by the Commissariat a l'Energie Atomique in the EDGAR-2 facility. [

] [a, c] The results are provided in Tables B.14-1 and B.14-2, and compared in Figure B.14-1 to the current ZIRLO™ model from Appendix C of Reference 3.

[

]$^{a, b, c}$

High-Temperature Oxidation

High-temperature oxidation measurements for Standard and Optimized ZIRLO™ were taken by UJP Praha. [

] $^{a, b, c}$ As shown in Figure B.15-1, the parabolic rate constants for the Baker-Just equation bound the Standard and Optimized ZIRLO™ data, confirming that the model required by 10 CFR 50 Appendix K remains conservative. Also, the ZIRLO™ best estimate parabolic rate constants from Equation 3 of Appendix E to Reference 3 bound the Standard and Optimized ZIRLO™ data at all three temperatures, indicating that the Best Estimate model is conservative relative to the new data. Based on these results, it is concluded that the current models for high-temperature oxidation can be applied to Optimized ZIRLO™ for Appendix K Large and Small Break LOCA and Best Estimate Large Break LOCA, and need not be modified to reflect the new Standard ZIRLO™ data. This conclusion is also considered to apply to SECY Large Break LOCA which, per Reference 9, uses the Baker-Just correlation for "Appendix K" calculations, and a ZIRLO™-specific model for "Superbounded" calculations.

Other LOCA Models

Appendix B provides test results for density, thermal expansion, Young's Modulus, and Poisson's Ratio which are also used in the Westinghouse LOCA codes. These properties were measured over limited temperature ranges, which is considered to be adequate given their minimal importance in typical licensing-basis Large and Small Break LOCA transients. Given this, and since the data indicate very little sensitivity to variations in tin content, the current Zircaloy-4/ZIRLO™ models for these parameters can reasonably be applied to Optimized ZIRLO™, and need not be modified to reflect the new Standard ZIRLO™ data.

4.6.2 CE ECCS Performance Evaluation Models

This section describes the implementation of Optimized ZIRLO™ in the Westinghouse Emergency Core Cooling System (ECCS) performance evaluation models for Combustion Engineering (CE) designed PWRs (herein referred to as the CE evaluation models).

Optimized ZIRLO™ is implemented in the following versions of the CE Large Break Loss-of-Coolant Accident (LBLOCA) and Small Break Loss-of-Coolant Accident (SBLOCA) evaluation models:

- Large Break LOCA: 1999 EM (Reference 10)
- Small Break LOCA: S2M (Reference 11)

These are the same versions of the CE evaluation models that have been NRC-accepted for analysis of Standard ZIRLO™ (Reference 5). Both the 1999 EM and the S2M are Appendix K evaluation models. The CE post-LOCA long term cooling evaluation model (Reference 12) does not use any cladding material property models. Consequently, it is not impacted by the implementation of Optimized ZIRLO™ and, therefore, is not addressed herein.

The LBLOCA and SBLOCA evaluation models contain models for the thirteen cladding properties listed in Table 4.6.2-1. Section 6.3 of Reference 5 describes the cladding models for Standard ZIRLO™ that are used in the CE evaluation models for LBLOCA and SBLOCA for each of the thirteen properties. Note that in many cases, as described in Section 6.3 of Reference 5, the models are the same as those that are used for Zircaloy-4 cladding.

Table 4.6.2-1
Cladding Properties Modeled in the CE Evaluation Models

Specific Heat	Thermal Expansion	Rupture Temperature
Density	Modulus of Elasticity	Rupture Strain
Thermal Conductivity	Poisson's Ratio	Assembly Blockage
Thermal Emissivity	Hardness	Pre-Rupture Plastic Strain
		Metal-Water Reaction Rate

The following sections address the impact of implementing Optimized ZIRLO™ on the thirteen cladding properties used in the LBLOCA and SBLOCA evaluation models. The Optimized ZIRLO™ and Standard ZIRLO™ test data, which are documented in Appendix B, are compared to the models for

Standard ZIRLO™ cladding that are used for each property in the CE evaluation models. Differences between the data and the models are noted and evaluated.

Specific Heat

The test data for the specific heat of Optimized ZIRLO™ and Standard ZIRLO™ are documented in Section B.2 of Appendix B. Data were generated for both heatup and cooldown transients [ ]$^{a, b, c}$ Section B.2 concludes that the specific heats of Optimized ZIRLO™ and Standard ZIRLO™ are equal within the accuracy of the data.

As described in Section 6.3.1 of Reference 5, the CE evaluation models represent the specific heat of Standard ZIRLO™ with a table of values as a function of temperature. Linear interpolation is used to calculate the specific heat for a given temperature. The table of values is documented in Table 6.3.1-2 of Reference 5. The same model is used for both cladding heatup and cooldown.

The Optimized ZIRLO™ and Standard ZIRLO™ data for heatup and cooldown are compared to the ZIRLO™ model in Figures 4.6.2-1 and 4.6.2-2, respectively. As observed in Figure 4.6.2-1, the heatup data and the model are in reasonable agreement in the alpha phase (less than approximately 1400°F) and the beta phase (greater than approximately 1700°F). In the phase transition temperature range where the heat of transformation is included in the specific heat, the data show [

]$^{a, b, c}$. The data and the model agree reasonably well in terms of the peak specific heat in the phase transition temperature range and the subsequent decrease as the values approach the specific heat of the beta phase.

As observed in Figure 4.6.2-2, the cooldown data exhibit [ ]$^{a, c}$ relative to the model for Standard ZIRLO™. [

]$^{a, b, c}$

Since a LOCA is primarily a heatup transient, the heatup data is the more important data set. As noted above, the Optimized ZIRLO™ data and the model for Standard ZIRLO™ are in good agreement over most of the temperature range. The exception is the low end of the alpha-to-beta phase transition

temperature range, from approximately 1400°F to 1600°F. The difference between the data and the model between 1400°F to 1600°F will impact the cladding heatup rate when the cladding temperature passes through that temperature range. However, the difference will not have a significant impact on the peak cladding temperature for LBLOCA and SBLOCA for the following reasons.

Figure 6.5.1.3-1 of Reference 5 shows a typical cladding temperature transient for the hot spot of the hot rod during a LBLOCA. The cladding heats up through the 1400°F-1600°F temperature range in approximately five seconds during blowdown and again in approximately fifteen seconds in early reflood. The peak cladding temperature occurs at approximately 250 seconds during late reflood. Since the model shows a greater specific heat than the data in the subject temperature range, the model will calculate a slower heatup rate during the two time periods that the temperature is in the subject temperature range. However, the cladding passes through the subject temperature range very quickly and the peak cladding temperature occurs significantly later in the transient when the cladding temperature is primarily controlled by the cladding-to-coolant heat transfer. As a result, if the experimentally determined values for specific heat were to be used in the evaluation model, the resultant increase in cladding temperature that would occur while the cladding is heating up through the subject temperature range would be small in magnitude and would decrease during the remainder of the reflood period. The result would be an insignificant change to the peak cladding temperature that is achieved in late reflood.

For reasons similar to those described above for the heatup data, the differences between the cooldown data and the model will also have an insignificant impact on peak cladding temperature. As shown in Figure 6.5.1.3-1 of Reference 5, prior to the peak cladding temperature, a period of cooldown only occurs for a brief period during blowdown.

The differences in specific heat will not have a significant impact on either the maximum or the core-wide cladding oxidation since the differences occur over a temperature range for which the rate of oxidation is low. Furthermore, as described above, there is only a small impact on cladding temperature within the temperature range.

Figure 6.5.2.3-1 of Reference 5 compares the hot spot cladding temperature transient for Standard ZIRLO™ and Zircaloy-4 cladding for a typical SBLOCA transient. In the case that is depicted, the location of the hot spot is not the elevation of cladding rupture. Since the cladding models that are different between Standard ZIRLO™ and Zircaloy-4 in the SBLOCA evaluation model are the models for specific heat, rupture temperature and rupture strain, the only meaningful difference between the two cases at the elevation depicted in Figure 6.5.2.3-1 is the difference in specific heat. The Standard

ZIRLO™ and Zircaloy-4 specific heat models are compared in Figure 6.3.1-1 of Reference 5. The difference between the two models is greater than the difference between the Optimized ZIRLO™ data and the Standard ZIRLO™ specific heat model (Figure 4.6.2-1). The difference in the peak cladding temperatures for the Standard ZIRLO™ and Zircaloy-4 cases depicted in Figure 6.5.2.3-1 of Reference 5 is 4°F. Because the difference between the specific heats of the Optimized ZIRLO™ data and the Standard ZIRLO™ model is smaller than the difference between the Standard ZIRLO™ and Zircaloy-4 specific heat models, the impact on peak cladding temperature of implementing an Optimized ZIRLO™ specific heat model rather than using the current Standard ZIRLO™ specific heat model in a SBLOCA analysis would be comparable to the difference shown in Figure 6.5.2.3-1 of Reference 5, i.e., approximately 4°F.

In summary, for the reasons described above, it is concluded that the model for the specific heat of Standard ZIRLO™ that is used in the CE evaluation models is acceptable for application to Optimized ZIRLO™ cladding.

Density

The test data for the density of Optimized ZIRLO™ and Standard ZIRLO™ are documented in Section B.1 of Appendix B. The data were obtained at room temperature. Section B.1 concludes that the data suggest a minor decrease in density with lower tin content.

As described in Section 6.3.2 of Reference 5, the CE evaluation models use a constant value of 409 lbm/ft^3 (6.552 gm/cm^3) for the density of Standard ZIRLO™. The same value is used for Zircaloy-4 cladding.

The experimentally determined values for Optimized ZIRLO™ and Standard ZIRLO™, which are listed in Table B.1-1 of Appendix B, are less than [ ]^{a,b,c} different from the value used in the CE evaluation models for Standard ZIRLO™. Section 6.3.2 of Reference 5 documents that a 2% difference in cladding density is insignificant in the CE evaluation models. On that basis, it is concluded that the value for the density of Standard ZIRLO™ that is used in the CE evaluation models is applicable to Optimized ZIRLO™ cladding.

Thermal Conductivity

The test data for the thermal conductivity of Optimized ZIRLO™ and Standard ZIRLO™ are documented in Section B.3 of Appendix B. [ ] [a,c]
Section B.3 concludes that the thermal conductivities of Optimized ZIRLO™ and Standard ZIRLO™ are indistinguishable within the accuracy of the data.

As described in Section 6.3.3 of Reference 5, the CE evaluation models use a [ ] [a, c] function of temperature for the thermal conductivity of Standard ZIRLO™. (The CEFLASH-4AS computer code uses a somewhat different [ ] [a, c] than the other evaluation model computer codes.) The models are the same as those used for Zircaloy-4 cladding.

The test data for Optimized ZIRLO™ and Standard ZIRLO™ are compared to the models used in the CE evaluation models in Figure 4.6.2-3. The data for Optimized ZIRLO™ compare very well with the models [

] [a, b, c]

This difference between the Optimized ZIRLO™ data and the model is comparable to the difference that is described in Section 6.3.3 of Reference 5 and is subsequently justified in the response to the Request for Additional Information (RAI) Question 10a in Reference 5. The justification is based on the fact that the thermal resistance of the cladding does not limit the fuel-to-coolant heat transfer during a LOCA. Consequently, differences in the cladding thermal conductivity of the subject magnitude do not significantly impact the cladding temperature transient. Therefore, based on the comparison and evaluation provided above, it is concluded that the models for the thermal conductivity of Standard ZIRLO™ that are used in the CE evaluation models are acceptable for application to Optimized ZIRLO™ cladding.

Thermal Emissivity

The test data for the thermal emissivity of oxidized zirconium alloys (Optimized ZIRLO™, Standard ZIRLO™, and Zircaloy-4) are documented in Section B.4 of Appendix B. Data were obtained [

] [a, b, c] Section B.4 concludes that the emissivity of Optimized ZIRLO™, Standard ZIRLO™, and Zircaloy-4 are indistinguishable within the accuracy of the data.

As described in Section 6.3.4 of Reference 5, the model for the thermal emissivity of Standard ZIRLO™ used in the CE evaluation models is a second order polynomial function of temperature. It is the same model that is used for Zircaloy-4 cladding.

The test data for Optimized ZIRLO™, Standard ZIRLO™, and Zircaloy-4 are presented in Figure B.4-1 of Appendix B. The test data for the three zirconium alloys indicate [

] [a, b, c]

As described in the discussion of emissivity in Section 4.6.1, emissivity is generally [

] [a, b, c] This value is comparable to the CE model for emissivity at high temperatures where rod-to-rod radiation becomes an important heat transfer mechanism.

As shown in Figure B.4-1, the test data show that the emissivity of Optimized ZIRLO™, Standard ZIRLO™, and Zircaloy-4 are reasonably similar when measured on a consistent basis, in this case, in a vacuum. Thus, the data do not give any reason to suggest that the emissivities of the three alloys would be dissimilar in the high temperature steam environment of a LOCA.

Base on the above, it is concluded that the model for the thermal emissivity of Standard ZIRLO™ that is used in the CE evaluation models is acceptable for application to Optimized ZIRLO™ cladding.

Thermal Expansion

The test data for the thermal expansion of Optimized ZIRLO™ and Standard ZIRLO™ are documented in Section B.5 of Appendix B. [

] [a, b, c] The data were used to define mean coefficients of thermal expansion for

[ ]^{a,b,c} The diametral coefficients range from [ ]^{a,b,c} Section B.5 concludes that the diametral thermal expansion of ZIRLO™ alloys is independent of tin content, with more than 90% confidence.

The CE evaluation models use diametral thermal expansion. The same model is used for both Standard ZIRLO™ and Zircaloy-4 cladding. The model is described in Section 6.3.5 of Reference 5. A least square linear fit to the heatup portion of the model [ ]^{a,b,c} gives a slope (i.e., coefficient of thermal expansion) of [ ]^{a,b,c}

Section 6.3.5 of Reference 5 describes a sensitivity study that demonstrated the insensitivity of peak cladding temperature to differences in thermal expansion at high temperature (>1500°F). The study calculated an insignificant change in peak cladding temperature [ ]^{a,b,c} for the change in thermal expansion that was investigated.

A similar sensitivity study was performed for Optimized ZIRLO™ to demonstrate that the peak cladding temperature is insensitive to differences in thermal expansion over the complete range of temperatures encountered during a LOCA. The study consisted of two cases. The first used the CE model for thermal expansion. The second used a single value of [ ]^{a,b,c} for the coefficient of thermal expansion. This value, which is greater than the largest Optimized ZIRLO™ value, was used for both heating and cooling and for all temperatures. The result was the same as the previous study; i.e., the peak cladding temperature changed by [ ]^{a,b,c}

Based on the results of the sensitivity study, it is concluded that the model for the thermal expansion of Standard ZIRLO™ that is used in the CE evaluation models is acceptable for application to Optimized ZIRLO™ cladding.

Modulus of Elasticity

The test data for the modulus of elasticity of Optimized ZIRLO™ and Standard ZIRLO™ are documented in Section B.7 of Appendix B. Data were obtained [

]^{a,b,c} Section B.7 concludes that the modulus of elasticities of Optimized ZIRLO™ and Standard ZIRLO™ are indistinguishable.

The CE evaluation models use a model for modulus of elasticity in the circumferential direction. The model, which is used for both Standard ZIRLO™ and Zircaloy-4, is described in Section 6.3.6 of Reference 5. The model consists of [

] [a, b, c] The model and the data for Optimized ZIRLO™ and Standard ZIRLO™ are in reasonable agreement over the temperature range covered by the data.

In providing the basis for the applicability of the Zircaloy-4 model for modulus of elasticity to Standard ZIRLO™ in the absence of any test data for Standard ZIRLO™, Section 6.3.6 of Reference 5 describes how variations in the modulus of elasticity between Standard ZIRLO™ and Zircaloy-4 will not have a significant impact on the cladding dimensions and, consequently, on the gap conductance, gap pressure, and cladding temperature. Based on those arguments and on the reasonable agreement between the test data and the model shown at low temperature, it is concluded that the model for the modulus of elasticity of Standard ZIRLO™ that is used in the CE evaluation models is acceptable for application to Optimized ZIRLO™ cladding.

Poisson's Ratio

The test data for Poisson's ratio for Optimized ZIRLO™ and Standard ZIRLO™ are documented in Section B.7 of Appendix B. Data were obtained [ ] [a, b, c] Section B.7 concludes that the Poisson's ratios for Optimized ZIRLO™ and Standard ZIRLO™ are indistinguishable.

As described in Section 6.3.7 of Reference 5, the model for Poisson's ratio used in the CE evaluation models consists of a linear equation [

] [a, b, c] The same model is used for both Standard ZIRLO™ and Zircaloy-4 cladding.

For the same reasons used for modulus of elasticity, Section 6.3.7 of Reference 5 reasoned that any differences in Poisson's ratio between Standard ZIRLO™ and Zircaloy-4 will have an insignificant impact on gap conductance and gap pressure and, hence, on the cladding temperature. Therefore, in the absence of any data, it was concluded that the model is acceptable for application to Standard ZIRLO™ cladding. Given the relative insensitivity of cladding temperature to variations in Poisson's ratio established in Reference 5, the same conclusion is reached for Optimized ZIRLO™ cladding. That is, the

model for Poisson's ratio that is used in the CE evaluation models for Standard ZIRLO™ is acceptable for application to Optimized ZIRLO™ cladding.

Hardness

The test data for the microhardness of Optimized ZIRLO™ and Standard ZIRLO™ are documented in Section B.8 of Appendix B. The data were obtained [

] [a, c] Section B.8 concludes that the difference in hardness between Optimized ZIRLO™ and Standard ZIRLO™ is minor.

The model for hardness that is used for Standard ZIRLO™ cladding in the CE evaluation models is described in Section 6.3.8 of Reference 5. It is the same model that is used for Zircaloy-4 cladding. The model consists of [

] [a, b, c]

The mean values listed in Table B.8-1 for the hardness of Optimized ZIRLO™ and Standard ZIRLO™ at room temperature differ from the value of [ ] [a, b, c] given by the CE evaluation model by [

.] [a, b, c]

In the CE evaluation models, cladding hardness is used in the calculation of the gap conductance when the fuel and cladding are in contact. Given the limited conditions under which the fuel and cladding are in contact during a LOCA, Section 6.3.8 of Reference 5 reasoned that any difference in hardness between Zircaloy-4 and Standard ZIRLO™ would have an insignificant impact on the gap conductance and, hence, on cladding temperature. Consequently, in the absence of hardness test data, it was concluded that the Zircaloy-4 cladding hardness model was suitable for application to Standard ZIRLO™ cladding. The room temperature data for Standard ZIRLO™ and Optimized ZIRLO™ support the continued applicability of that conclusion. Therefore, it is concluded that the model for the hardness of Standard ZIRLO™ that is used in the CE evaluation models is acceptable for application to Optimized ZIRLO™ cladding.

Rupture Temperature

The test data for the rupture temperature of Optimized ZIRLO™ cladding are documented in Section B.13 of Appendix B. Data were [

] [a, b, c] Section B.13 concludes that the data for Optimized ZIRLO™ are indistinguishable from the original data for Standard ZIRLO™.

As described in Section 6.3.9 of Reference 5, the model for the rupture temperature of Standard ZIRLO™ cladding that is used in the CE evaluation models is a table of rupture temperature versus engineering hoop stress.

Figure B.13-2 compares the test data to the model. The agreement between the data and the model is similar to the agreement between the original Standard ZIRLO™ test data that was used to develop the model and the model (Figure D-1 of Reference 1).

Based on the agreement between the Optimized ZIRLO™ test data and the Standard ZIRLO™ model, it is concluded that the model for the rupture temperature of Standard ZIRLO™ cladding that is used in the CE evaluation models is applicable to Optimized ZIRLO™ cladding.

Rupture Strain

The test data for the circumferential rupture strain of Optimized ZIRLO™ cladding are documented in Section B.13 of Appendix B. Data were obtained [

] [a, b, c] Section B.13 concludes that the data for Optimized ZIRLO™ are indistinguishable from the original data for Standard ZIRLO™.

As described in Section 6.3.10 of Reference 5, the model for the circumferential rupture strain of Standard ZIRLO™ cladding that is used in the CE evaluation models is a table of circumferential rupture strain versus rupture temperature.

Figure B.13-1 compares the test data to the model. The agreement between the data and the model is similar to the agreement between the original Standard ZIRLO™ test data that was used to develop the model and the model (Figure D-6 of Reference 1).

Based on the agreement between the Optimized ZIRLO™ test data and the Standard ZIRLO™ model, it is concluded that the model for the circumferential rupture strain of Standard ZIRLO™ cladding that is used in the CE evaluation models is applicable to Optimized ZIRLO™ cladding.

Assembly Blockage

As described in Section 6.3.11 of Reference 5, the assembly blockage model for Standard ZIRLO™ cladding that is used in the CE evaluation models was developed from the rupture strain model using the geometric conversion methodology from NUREG-0630 (Reference 13). Since it was concluded above that the Standard ZIRLO™ rupture strain model is applicable to Optimized ZIRLO™ cladding, it follows that the Standard ZIRLO™ assembly blockage model is also applicable to Optimized ZIRLO™ cladding.

The Standard ZIRLO™ assembly blockage model, which consists of a table of assembly blockage as a function of rupture temperature, is documented in Table 6.3.11-1 of Reference 5.

Pre-Rupture Plastic Strain

The CE LBLOCA evaluation model uses a pre-rupture plastic strain (i.e., high temperature creep) model that calculates plastic strain as a function of cladding temperature, cladding rupture temperature, and cladding rupture strain. The model was prescribed by the NRC during the initial review of the CE LBLOCA evaluation model and, hence is referred to as the "NRC model". It is used in STRIKIN-II to determine the inside diameter of the cladding that is used in the calculation of the fuel-to-cladding gap conductance and in the calculation of the fuel rod internal pressure. The model is also used in the CEFLASH-4A dynamic fuel rod internal pressure model. Because the results of SBLOCA analyses are less sensitive to the fuel-to-cladding gap conductance, the CE SBLOCA evaluation model does not use a plastic strain model.

As described in Section 6.3.12 of Reference 5, the NRC model is applied to Standard ZIRLO™ cladding with no changes to the model itself. When the model is applied to Standard ZIRLO™ cladding, the Standard ZIRLO™ models for rupture temperature and rupture strain are used to determine the cladding rupture temperature and rupture strain in the above equation.

The results of the Optimized ZIRLO™ high temperature creep tests are presented in Section B.14 of Appendix B and are further discussed in Section 4.6.1. Section 4.6.1 concludes that the Optimized ZIRLO™ and Standard ZIRLO™ data are [

]$^{a, b, c}$ Similarly, it is judged that the pre-rupture plastic strain model that is used in the CE LBLOCA evaluation model for Standard ZIRLO™ (i.e., the NRC model) is acceptable for application to Optimized ZIRLO™ cladding.

Metal-Water Reaction Rate

The test data for the high temperature metal-water reaction rate for Optimized ZIRLO™ and Standard ZIRLO™ are documented in Section B.15 of Appendix B. [

] [a, b, c]

Parabolic reaction rates were calculated [ ] [a, c] for each material lot. Section B.15 concludes that all the test data fall well below the Baker-Just metal-water reaction rate model.

The CE evaluation models use the Baker-Just metal-water reaction rate model for Standard ZIRLO™ cladding. Applicability of the Baker-Just model to Standard ZIRLO™ cladding is described in Section 6.3.13 of Reference 5.

Figure B.15-1 compares the parabolic reaction rate constants calculated from the test data to the Baker-Just model. The comparison shows that the Baker-Just model predicts higher reaction rate constants than those calculated for Optimized ZIRLO™. Based on this comparison, it is concluded that the Baker-Just model is conservatively applicable to Optimized ZIRLO™ cladding.

Summary

The previous sections compare and evaluate the Optimized ZIRLO™ test data relative to the corresponding cladding models for Standard ZIRLO™ that are used in the CE evaluation models. The evaluations conclude that the models used for Standard ZIRLO™ are acceptable for application to Optimized ZIRLO™ cladding in ECCS performance analyses using the CE evaluation models.

Figure 4.6.2-1
Specific Heat (Heatup) Comparison of Test Data and CE Evaluation Model

[a, b, c

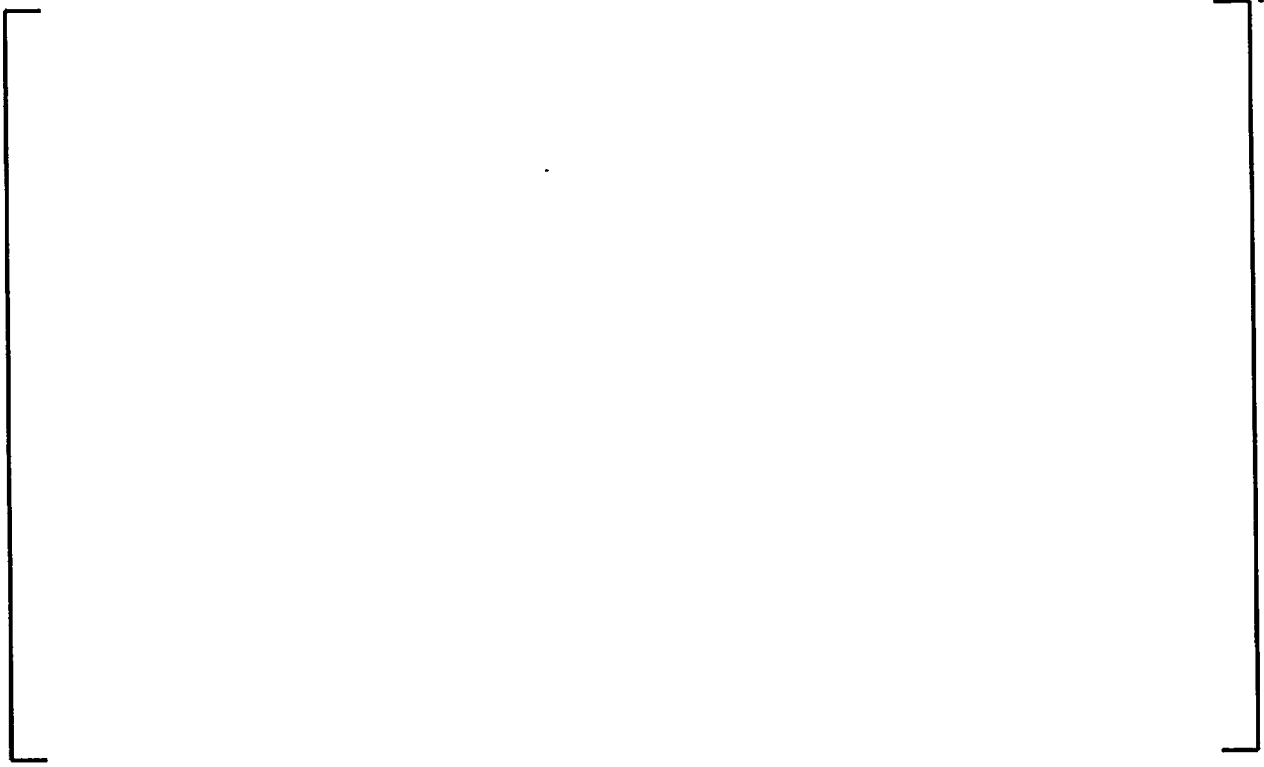

]

Figure 4.6.2-2
Specific Heat (Cooldown) Comparison of Test Data and CE Evaluation Model

a, b, c

Figure 4.6.2-3
Thermal Conductivity Comparison of test Data and CE Evaluation Model

a, b, c

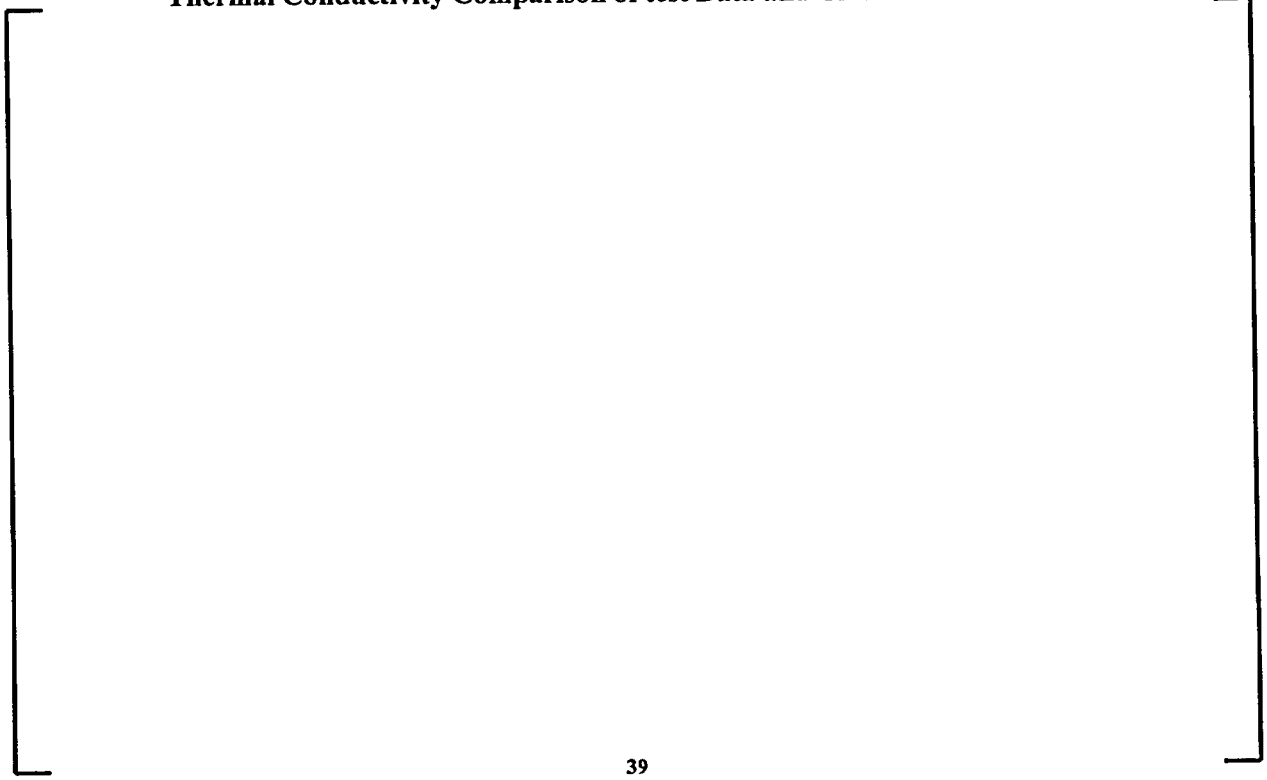

4.6.3 Applicability of 10 CFR 50.46 to Optimized ZIRLO™

Ring compression tests were performed on Optimized ZIRLO™ and Standard ZIRLO™ to assess the retained ductility of the cladding following oxidation in high temperature steam at conditions up to and beyond the maximum cladding oxidation and peak cladding temperature requirements specified in 10 CFR50.46. The results show that the retained ductility of Optimized ZIRLO™ is equivalent to that of Standard ZIRLO™. Therefore, the 10 CFR 50.46 requirements applicable to Standard ZIRLO™ are also applicable to Optimized ZIRLO™. Details of the testing methods and results are provided in the Appendices A and B.

4.7 Radiological

As documented in the original submittal to the NRC[3], the introduction of ZIRLO™ cladding did not have any appreciable effect on source terms and radiological dose analyses. The principal radiological effect that was discussed, was related to the increased burnup of the fuel from 60 GWD/MTU to 75 GWD/MTU. Even though Reference 3 was only licensed by the NRC to 60 GWD/MTU, the evaluations/analyses performed in support of that submittal would still be considered bounding for the application of Optimized ZIRLO™, which is requested to be licensed by the NRC to 62 GWD/MTU.

The original source terms and radiological analyses assumed Zircaloy-4 as a cladding material. Reference 3 introduced ZIRLO™ cladding and this addendum discusses the Optimized ZIRLO™ product. In reviewing the constituent makeup of ZIRLO™ or Optimized ZIRLO™, the addition of a nominal amount of niobium has a negligible effect on source terms or dose analyses. The reduction in tin content, in the Optimized ZIRLO™, will have no impact on source terms or dose analyses.

5.0 Conclusions

Extensive characterization tests performed on Standard and Optimized ZIRLO™ verify that the minor material composition change does not appreciably change the ZIRLO™ physical, mechanical, microstructural or LOCA properties. Therefore, the minor composition change also does not have any impact on analysis models and methods. Standard ZIRLO™ material properties currently utilized in various models and methodologies will be applied to analyses of Optimized ZIRLO™.

6.0 References

1. Letter from W. J. Johnson (Westinghouse) to V. H. Wilson (NRC), "WCAP-12610, VANTAGE + Fuel Assembly Reference Core Report (Proprietary)," NS-NRC-90-3519, June 13, 1990.

2. Letter from A. C. Thadani (NRC) to S. R. Tritch (Westinghouse), "Acceptance for Referencing of Topical Report WCAP-12610 'VANTAGE + Fuel Assembly Reference Core Report'," TAC. NO. 77258, July 1, 1991.

3. Davidson, S. L. (Ed.), et al., "VANTAGE + Fuel Assembly Reference Core Report," WCAP-12610-P-A, April 1995.

4. "Use of Fuel with Zirconium-Based (Other than Zircaloy) Cladding (10 CFR 50.44, 50.46, and Appendix K to Part 50)," Federal Register, Vol. 57, No. 169, Rules and Regulations, pg. 39353 and 39355, August 31, 1992.

5. "Implementation of ZIRLO™ Cladding Material in CE Nuclear Power Fuel Assembly Designs," CENPD-404-P-A, Revision 0, November 2001.

6. Davidson, S. L. (Ed.), et al., "Reference Core Report 17x17 Optimized Fuel Assembly," WCAP-9500-A, May 1982.

7. Davidson, S. L. and Kramer, W. R., "Reference Core Report VANTAGE 5 Fuel Assembly," WCAP-10444-P-A, September 1985.

8. "SCDAP/RELAP5/MOD 3.3 Code Manual: MATPRO - A Library of Materials Properties for Light-Water-Reactor Accident Analysis," NUREG/CR-6150, Volume 4, Revision 2, INEL-96/0422, January 2001.

9. Spaargaren, J. S., "10 CFR 50.46 Evaluation Model Report: WCOBRA/TRAC Two-Loop Upper Plenum Injection Model Updates to Support ZIRLO™ Cladding Option," WCAP-13677-P-A, February 1994.

10. "Calculative Methods for the CE Nuclear Power Large Break LOCA Evaluation Model," CENPD-132, Addendum 4-P-A, March 2001.

11. "Calculative Methods for the ABB CE Small Break LOCA Evaluation Model," CENPD-137, Addendum 2-P-A, April 1998.

12. "Post-LOCA Long Term Cooling Evaluation Model," CENPD-254-P-A, June 1980.

13. NUREG-0630, "Cladding Swelling and Rupture Models for LOCA Analysis," April 1980.

APPENDIX A
TEST METHODS

Physical Properties

A.1 Density:

Procedure/Technique: The immersion density method was used to experimentally determine the densities of the two tin levels of the Optimized ZIRLO™. The density of each specimen was calculated using the following equation,

$$\rho = (W_{air} * \rho_{solution})/(W_{air} - W_{solution})$$

where:

ρ = Density of the specimen
$\rho_{solution}$ = Density of the solution
W_{air} = Weight of the specimen in air
$W_{solution}$ = Weight of the specimen in the solution

A.2 Specific Heat:

Procedure/Technique: Measurements were made using the methods of ASTM E1269-01, Differential Scanning Calorimetry. The sample is heated electrically at a set rate, measured by thermocouple, and the heat input required to achieve the desired rate is recorded.

A.3 Thermal Conductivity:

Procedure/Technique: In order to determine thermal conductivity, thermal diffusivity was measured by the methods of ASTM E1461 in which one side of a disk-shaped sample is heated with a laser pulse of known energy and the temperature on the back side of the sample is measured with an infrared sensor. The sample is preheated to the desired base temperature in a furnace. The temperature rise on the front face is [ ]$^{a, b, c}$ on the back face. The thermal diffusivity is calculated from the temperature-time profile on the back of the specimen, and converted to thermal conductivity according to the equation,

$$\lambda = \kappa \rho c_p$$

where

λ = thermal conductivity
κ = thermal diffusivity
ρ = density; and
c_p = specific heat, with heats of transformation subtracted out.

A.4 Emissivity:

Procedure/Technique: Hemispherical total emissivity was measured by passing a current through a tubular sample in vacuum ($p < 1$ mPa) to heat it, measuring the temperature with an embedded thermocouple, surrounding it with a chilled, blackened bell jar, and calculating the heat input necessary to maintain the temperature. This is consistent with the ASTM method (C835-00), except that a tubular specimen was used instead of a strip. It is judged that the difference in shape had minimal effect on the results, whereas it allowed the tests to be performed on standard material. The temperature range accessible was limited by the tendency of the ends of the samples to reach a higher temperature than the center, so that chemical interactions between the specimen and the holders occurred when the test region was at relatively low temperatures.

A.5 Thermal Expansion (Dilatometry):

Procedure/Technique: The dilatometer measures the dimensional change of the specimen as a function of temperature. Axial test specimens were nominally 2 inches long (51 mm). For diametral measurements, half inch long samples were placed adjacent to each other to obtain a nominal gauge length of 47.5 mm. For some of the diametral measurements, the stability of the stack was increased by placing an Inconel rod though holes drilled in the tube sections.

The specimens were heated at a rate of 3 °C/minute and the length change was monitored by a digital transducer at the end of a push rod in contact with the specimen. Data were collected at 30-second intervals or about every 1.5 °C. The resolution of the digital transducer was 0.001 mm (1 μm). The specimen was heated in a closed system that was evacuated and backfilled with argon. A small flow of argon was maintained during the measurement to minimize oxidation of

the sample. [

]$^{a, b, c}$

The system was calibrated by running a sapphire reference sample from Anter Corporation. The calibration run was conducted using the same parameters that were used during measurement of the test specimens (i.e., heating and cooling rates of 3 °C/minute). Deviation between the measured expansion and book value for the sapphire expansion was attributed to the system expansion. This deviation was then used to correct the measured expansion of the Zr alloy samples for system expansion.

$$(\Delta L/L)_{corrected} = (\Delta L/L)_{measured} + Deviation$$

A.6 Phase Transition Temperature:

Procedure/Technique: This analysis used data from deviations from smooth curves in the dilatometry (described above) and in the specific heat measurements (also described above) to determine the phase transition temperatures.

A.7 Mechanical Tests:

Procedure/Technique: Mechanical tests were performed on [ ]$^{a, b, c}$ lots of ZIRLO™ cladding with nominal tin content ranging from [ ]$^{a, b, c}$ w/o. Test temperatures were [ ]$^{a, b, c}$ Measured properties include elastic modulus, Poisson's ratio (temperature ≤ 200 °C), 0.2% offset yield stress, ultimate stress and total elongation.

Testing was performed on a 50,000-pound Instron (Model 1127) tensile machine. An extensometer was attached to the 2-inch gauge section of the tubes to monitor sample elongation. Load versus elongation was recorded on two x-y chart recorders. One chart recorder measured the yield portion of the tensile curve and was used for determining the elastic modulus and 0.2% offset yield. The second chart recorder measured the full load versus elongation curve and provided the ultimate load and total elongation.

Poisson's ratio was measured for the low temperature tests (RT and 200 °C). A stain gauge (Micro-Measurements WK-03-125CA-350) was attached to the specimen to measure diametral strain while the extensometer measured axial displacement over the 2-inch gauge length. Poisson's ratio was determined from the slope of the diametral strain versus axial displacement curve.

Strain rate was controlled by the crosshead speed of the tensile machine. For selected samples, axial displacement over the 2-inch gauge was recorded as a function of time with the slope of the curve being proportional to strain rate. These curves were used to determine strain rates through the 0.2% offset yield and through uniform elongation to determine appropriate crosshead speeds to meet the test requirement of < 0.2%/minute through 1% strain and < 2%/minute for strains greater than 1%.

The hoop tests were based on two articles published in The Journal of Testing and Evaluation which describe a split-D type procedure. Testing was performed on a 50,000-pound servohydraulic testing machine. Specialized tooling and extensometer were developed in-house. Load, time, and displacement were recorded digitally with the testing system controller.

A.8 Microhardness Test:

Procedure/Technique: A Vickers microhardness test (ASTM E384-99e1) was performed by pressing an indenter of standardized shape into the specimen with a known force, and measuring the size of the indentation. Because it measures a very small region of the sample, it is useful in determining the uniformity of mechanical properties through the thickness of a tube wall or strip. The data reported here were measured on either surfaces parallel to the long axis of the tube ("longitudinal") or perpendicular to the long axis ("transverse").

A.9 Creep:

Procedure/Technique: The thermal creep test was performed at 725 °F, at an effective stress of 15.6 ksi, for a total of 40 days. The test was conducted in accordance with Westinghouse internal procedures.

A.10 Fatigue:

Procedure/Technique: The test was performed using push and pull loading conditions in the tube axial direction and conducted in accordance with Westinghouse internal procedures. [

]$^{a, b, c}$

A.11 Texture:

Procedure/Technique: Direct x-ray pole measurements were made at mid-wall, inner and outer diameter locations. The measurements were made in accordance with Westinghouse internal procedures.

A.12 Corrosion:

Procedure/Technique: The alloys were corrosion tested in 680 °F water and 800 °F steam environments. The water test was conducted in accordance with the ASTM G2 while the 800 °F steam tests were performed in accordance with Westinghouse internal procedures.

A.13 Single Rod Burst Test:

Procedure/Technique: Westinghouse performed high temperature burst tests on ZIRLO™ cladding samples in the late 1980s. Upon completion of the tests and over time, the original test equipment has been dismantled and scrapped. To perform the high temperature burst tests on the current materials, a new test facility was designed and built. The new burst test facility and procedures were designed to minimize any differences from the prior ZIRLO™ test program. Axial and azimuthal temperature measurements taken as part of the facility qualification indicated that the new facility would be capable of closely replicating the prior burst test results. This was confirmed by performing burst tests with control samples of standard ZIRLO™ tubing.

Each single rod burst test was conducted using [

]$^{a, b, c}$ The burst temperature for each sample was recorded, and the circumference at the rupture location was measured for use in calculating the circumferential burst strain.

A.14 High Temperature Creep Test:

Procedure/Technique: The French Commissariat a l'Energie Atomique (CEA) in Saclay, France using the EDGAR-2 facility performed the creep tests. Individual samples of cladding were inductively heated to the test temperatures in steam and pressurized with argon. The system pressure was controlled such that a constant hoop stress state was maintained within the cladding. The change in diameter of the cladding was monitored by a laser measurement device and periodic readings were recorded as a function of time.

Plots of the diametral strain as a function of time were analyzed. The slope of a line originating at zero strain, drawn tangent to strain versus time curve produces a creep rate for each hoop stress and temperature combination at 1183 °K or

lower. For Tests at 1273 °K the secondary phase of creep was measured. The creep rates as a function of hoop stress are reported in Appendix B of this report. The solid lines represent the results obtained for Standard ZIRLO™ as part of the initial ZIRLO™ licensing effort (as reported in Appendix C of Reference 3).

A.15 Metal Water Reaction Test:

Procedure/Technique: [ ]^{a,b,c} lots of Optimized ZIRLO™ samples were tested, along with one lot of Standard ZIRLO™ for control and comparison purposes. 1.5-inch long samples of cladding were prepared from each material lot. The sample dimensions were measured and the pre-oxidized masses were noted. [

]^{a,b,c} The oxidized mass of each sample, exposure temperature, and the exposure time were recorded for each sample.

A parabolic reaction rate for each temperature was then calculated using a series of plots and linear fits. The measured mass gains for each temperature were squared and then plotted as a function of time. This results in a linear relationship between mass gained from oxidation as a function of time. A linear regression analysis on this data provides a slope value that corresponds to a parabolic reaction rate. This reaction rate defines the relationship between exposure time and oxide formation. This analysis was repeated for each material at each of the [ ]^{a,b,c} oxidizing temperatures.

A.16 Ring Compression Test:

Procedure/Technique: A collection of oxidized Standard ZIRLO™ and Optimized ZIRLO™ samples that were prepared as part of the metal-water reaction analysis were submitted for ring compression testing. Ring samples were taken from oxidation specimens with targeted ECR values of [ ]^{a,b,c}

The tests were performed at 275 °F. The load and deflection data were then analyzed to determine the retained ductility of the cladding.

APPENDIX B
TEST RESULTS

Physical Properties

B.1 Density:

Results: The densities of each alloy were calculated based on weight measurements of each sample in air and immersed in water using the formula described in Appendix A. The results are tabulated in the table below. The result suggests a minor decrease in density with lower tin content. The new measured densities are slightly higher compared to the value, [ ]$^{a, b, c}$ reported previously. This small difference may be due to differences in equipment sensitivity and experimental procedure.

Table B.1-1
Density of Standard and Optimized ZIRLO™

a, b, c

[ ]

Table B.1-2 (cont.)
Detailed Sampling of Standard and Optimized ZIRLO™ for Density

[a, b, c

]

B.2 Specific Heat:

Results: [

]a, b, c

Within the accuracy of this data, the specific heats of Standard ZIRLO™ and Optimized ZIRLO™ are equal.

[

]a, b, c

Figure B.2-1
Specific Heat of Standard and Optimized ZIRLO™ on Heating

[a. b. c

]

Figure B.2-2
Specific Heat of Standard and Optimized ZIRLO™ on Cooling

[a, b, c

]

Table B.2-1
Specific Heat of Standard and Optimized ZIRLO™ on Heating and Cooling

a, b, c

[

]

Table B.2-1 (cont.)
Specific Heat of Standard and Optimized ZIRLO™ on Heating and Cooling a, b, c

Table B.2-1 (cont.)
Specific Heat of Standard and Optimized ZIRLO™ on Heating and Cooling

a, b, c

[

]

Table B.2-1 (cont.) a, b, c

Specific Heat of Standard and Optimized ZIRLO™ on Heating and Cooling

Table B.2-1 (cont.)
Specific Heat of Standard and Optimized ZIRLO™ on Heating and Cooling

a, b, c

[ ]

B.3 Thermal Conductivity:

Results: Thermal diffusivity is shown in Figure B.3-1 and thermal conductivity in Figure B.3-2. Within the accuracy of this data, thermal transport properties (diffusivity and conductivity) of Standard ZIRLO™ and Optimized ZIRLO™ are indistinguishable, as would be expected.

Figure B.3-1
Thermal Diffusivity of Standard and Optimized ZIRLO™

a, b, c

[ ]

Figure B.3-2
Thermal Conductivity of Standard and Optimized ZIRLO™

a, b, c

[ ]

Table B.3-1
Thermal Diffusivity and Conductivity of Standard and Optimized ZIRLO™

a, b, c

[ ]

B.4 Emissivity:

Results: The measurements are shown in Figure B.4-1. Within the accuracy of this data, the emissivity of Standard ZIRLO™, Optimized ZIRLO™, and Zircaloy-4 are indistinguishable. Emissivity measurement uncertainty is estimated as ± 2%.

Figure B.4-1
Thermal Emissivity of Oxidized Zirconium Alloys

a, b, c

[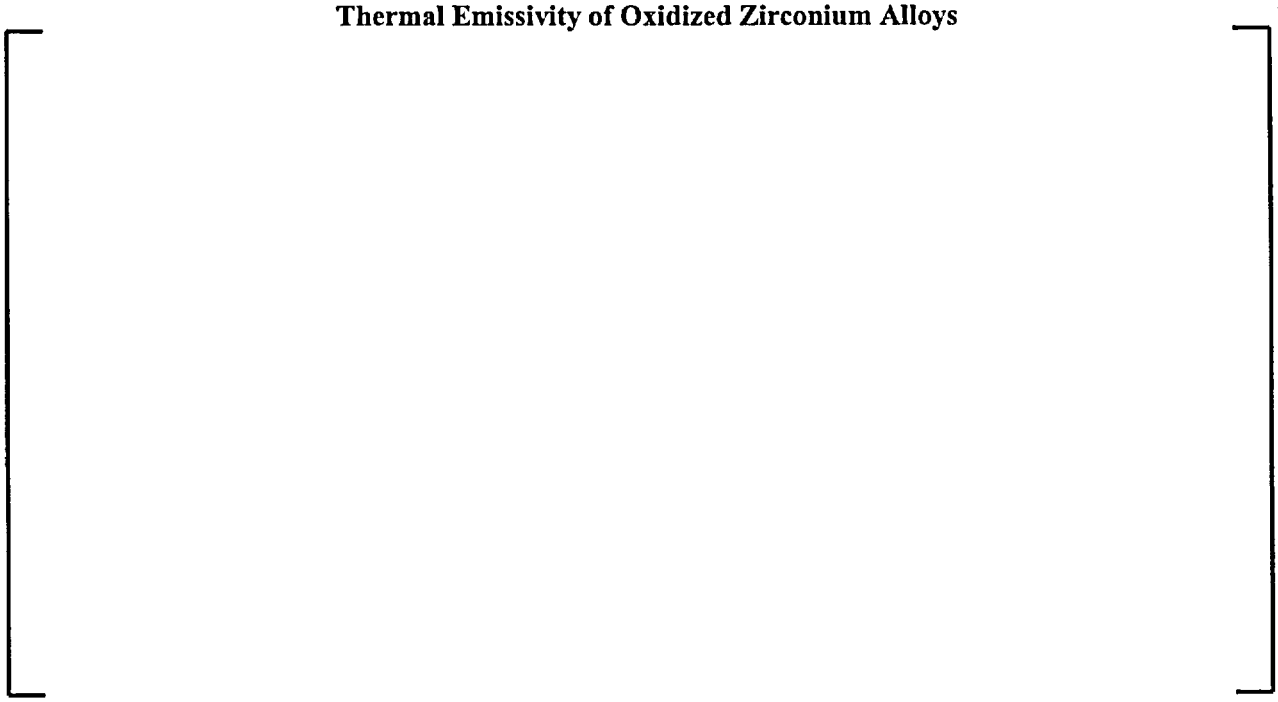]

Table B.4-1
Thermal Emissivity of Oxidized Zirconium Alloys

a, b, c

[ ]

B.5 Thermal Expansion (Dilatometry):

Results: The axial thermal expansion of ZIRLO™ from room temperature to 500 °C is independent of tin content for the materials tested, with more than 99% confidence.

The diametral thermal expansion of ZIRLO™ from room temperature to 500 °C is independent of tin content for the materials tested, with more than 90% confidence.

a, b, c

[ ]

Figure B.5-1
Axial Thermal Expansion Curve

a, b, c

[ ]

Table B.5-1
Axial Thermal Expansion Data

a, b, c

[ ]

Table B.5-1 (cont.)
Axial Thermal Expansion Data

a, b, c

Table B.5-1 (cont.)
Axial Thermal Expansion Data

a, b, c

Table B.5-1 (cont.)
Axial Thermal Expansion Data

a, b, c

Table B.5-1 (cont.)
Axial Thermal Expansion Data

a, b, c

Table B.5-1 (cont.)
Axial Thermal Expansion Data

a, b, c

[

]

Table B.5-1 (cont.)
Axial Thermal Expansion Data

a, b, c

Table B.5-1 (cont.)
Axial Thermal Expansion Data

[a, b, c]

Table B.5-1 (cont.)
Axial Thermal Expansion Data

a, b, c

Table B.5-1 (cont.)
Axial Thermal Expansion Data

a, b, c

Table B.5-1 (cont.)
Axial Thermal Expansion Data

a, b, c

Table B.5-1 (cont.)
Axial Thermal Expansion Data

a, b, c

Table B.5-1 (cont.)
Axial Thermal Expansion Data

a, b, c

[

]

Table B.5-1 (cont.)
Axial Thermal Expansion Data

a, b, c

[

]

Table B.5-1 (cont.)
Axial Thermal Expansion Data

a, b, c

Table B.5-1 (cont.)
Axial Thermal Expansion Data

a, b, c

a, b, c

Figure B.5-2
Typical Diametral Thermal Expansion Curve

[

]

Table B.5-2

Diametral Thermal Expansion Data

a, b, c

[

]

a, b, c

[

]

Table B.5-2 (cont.)
Diametral Thermal Expansion Data

[a, b, c]

Table B.5-2 (cont.)
Diametral Thermal Expansion Data

[a, b, c]

Table B.5-2 (cont.)
Diametral Thermal Expansion Data

a, b, c

[

]

Table B.5-2 (cont.)
Diametral Thermal Expansion Data

a, b, c

[

]

Table B.5-2 (cont.)
Diametral Thermal Expansion Data

a, b, c

Table B.5-2 (cont.)
Diametral Thermal Expansion Data

[a, b, c]

Table B.5-2 (cont.)
Diametral Thermal Expansion Data

[a, b, c]

Table B.5-2 (cont.)
Diametral Thermal Expansion Data

[a, b, c]

Table B.5-2 (cont.)
Diametral Thermal Expansion Data

[a, b, c]

Table B.5-2 (cont.)
Diametral Thermal Expansion Data

a, b, c

Table B.5-2 (cont.)
Diametral Thermal Expansion Data

a, b, c

Table B.5-2 (cont.)
Diametral Thermal Expansion Data

a, b, c

Table B.5-2 (cont.)
Diametral Thermal Expansion Data

a, b, c

Table B.5-2 (cont.)
Diametral Thermal Expansion Data

a, b, c

Table B.5-2 (cont.)
Diametral Thermal Expansion Data

[a, b, c]

B.6 Phase Transition Temperature:

Results: Phase transition temperatures are determined from a break in the curve of some property which is known to show a discontinuous change across phase transitions. For the present work, [

.]$^{a, b, c}$

[a, b, c

]

Figure B.6-1
$\alpha \leftrightarrow \alpha + \beta$ Phase Transition as a Function of Tin Content in ZIRLO™

a, b, c

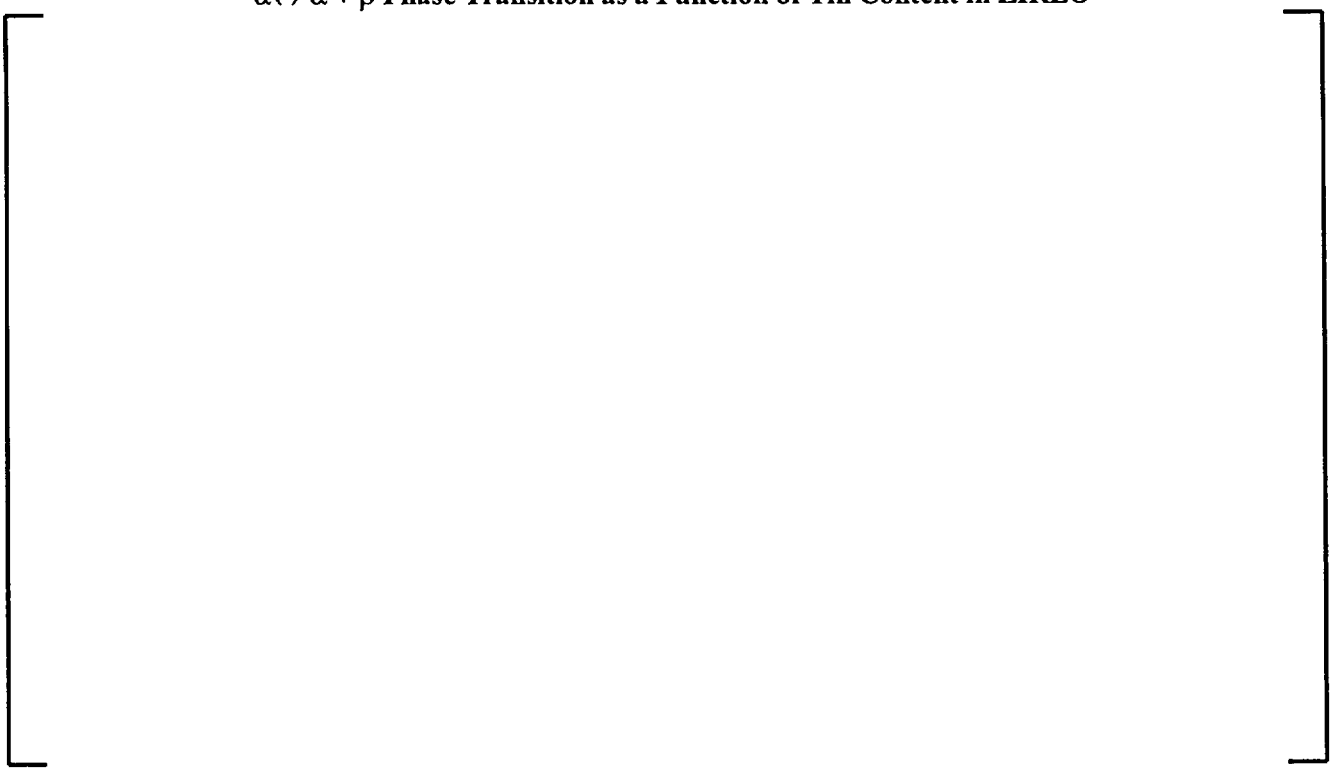

Table B.6-1
$\alpha \leftrightarrow \alpha + \beta$ Phase Transition as a Function of Tin Content in ZIRLO™

a, b, c

[

]

B.7 Mechanical Test:

a, b, c

Results: [

]

In measures of ductility (total elongation in the longitudinal direction, failure strain circumferentially), Optimized and Standard ZIRLO™ are indistinguishable at temperatures above room temperature.

In elastic properties (longitudinal and circumferential Young's modulus and circumferential/longitudinal Poisson's ratio), Optimized and Standard ZIRLO™ are indistinguishable.

Figure B.7-1
Longitudinal Yield Stress of ZIRLO™ with Three Tin Levels

a, b, c

Figure B.7-2
Longitudinal Ultimate Tensile Stress of ZIRLO™ with Three Tin Levels

a, b, c

a, b, c

Figure B.7-3
Longitudinal Total Elongation of ZIRLO™ with Three Tin Levels

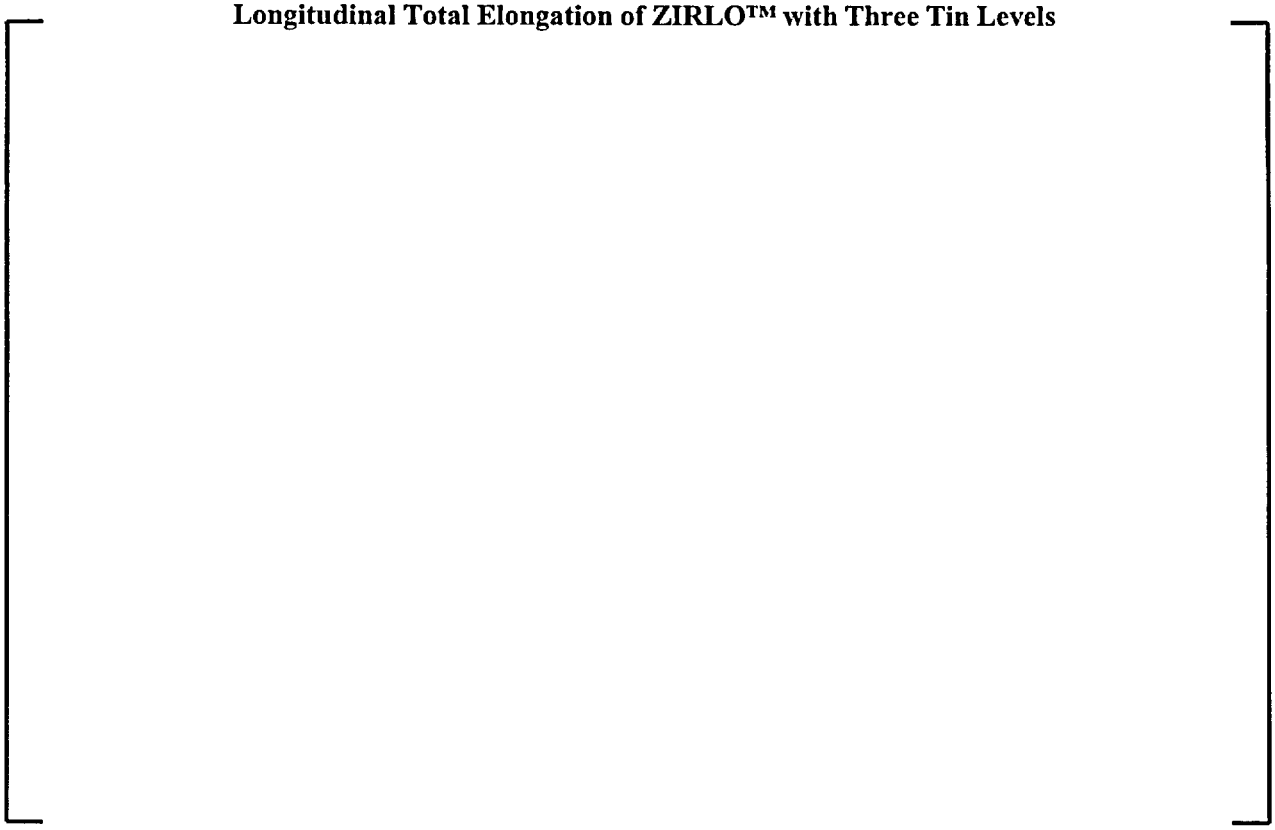

Figure B.7-4

Longitudinal Young's Modulus of ZIRLO™ with Three Tin Levels

a, b, c

Figure B.7-5

Poisson's Ratio, Hoop/Longitudinal, of ZIRLO™ with Three Tin Levels

a, b, c

Figure B.7-6
Circumferential Yield Stress

Figure B.7-7
Circumferential Failure Stress

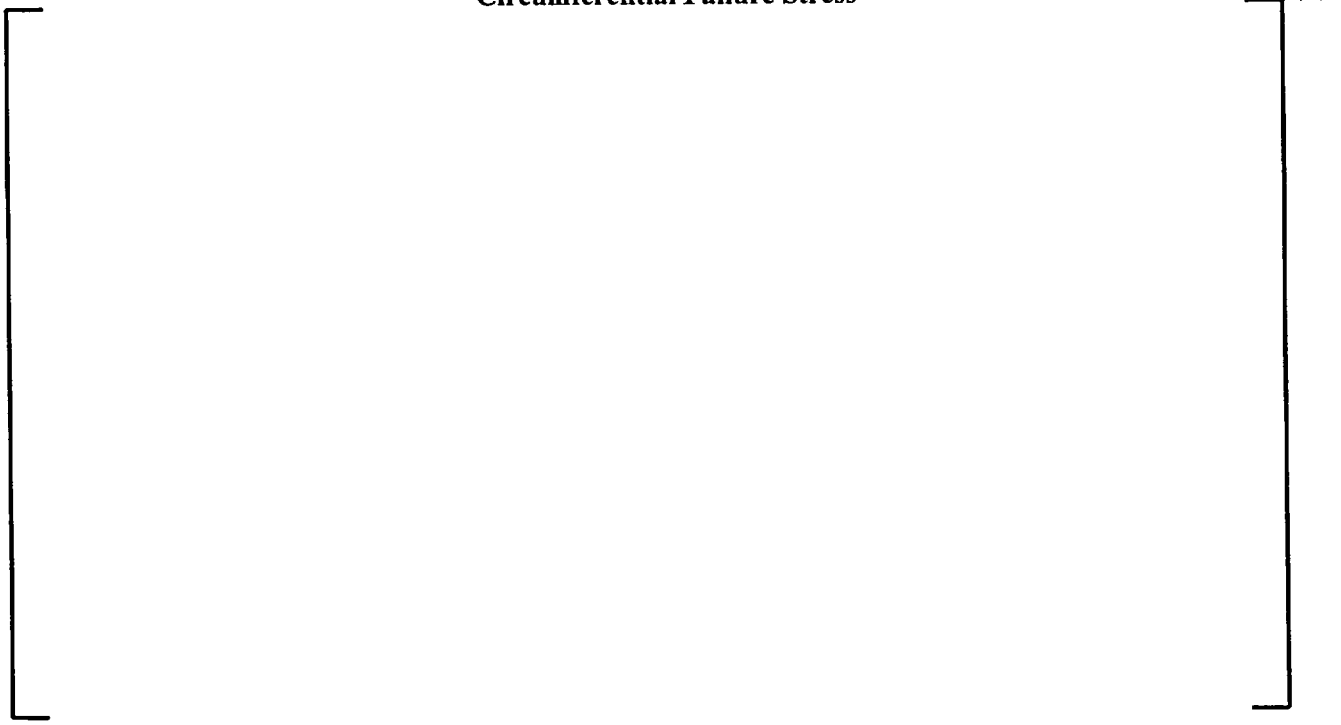

Figure B.7-8
Circumferential Failure Strain

a, b, c

Figure B.7-9
Circumferential Young's Modulus

a, b, c

Table B.7-1
Tensile Data

a, b, c

[

]

Table B.7-1 (cont.)
Tensile Data

[a, b, c

]

B.8 Microhardness Test:

Results: The results are plotted in Figures B.8-1 and B.8-2. The difference between the Optimized ZIRLO™ and the Standard ZIRLO™ is minor.

[

]a, b, c

[

]a, b, c

Figure B.8-1
Longitudinal Microhardness

a, b, c

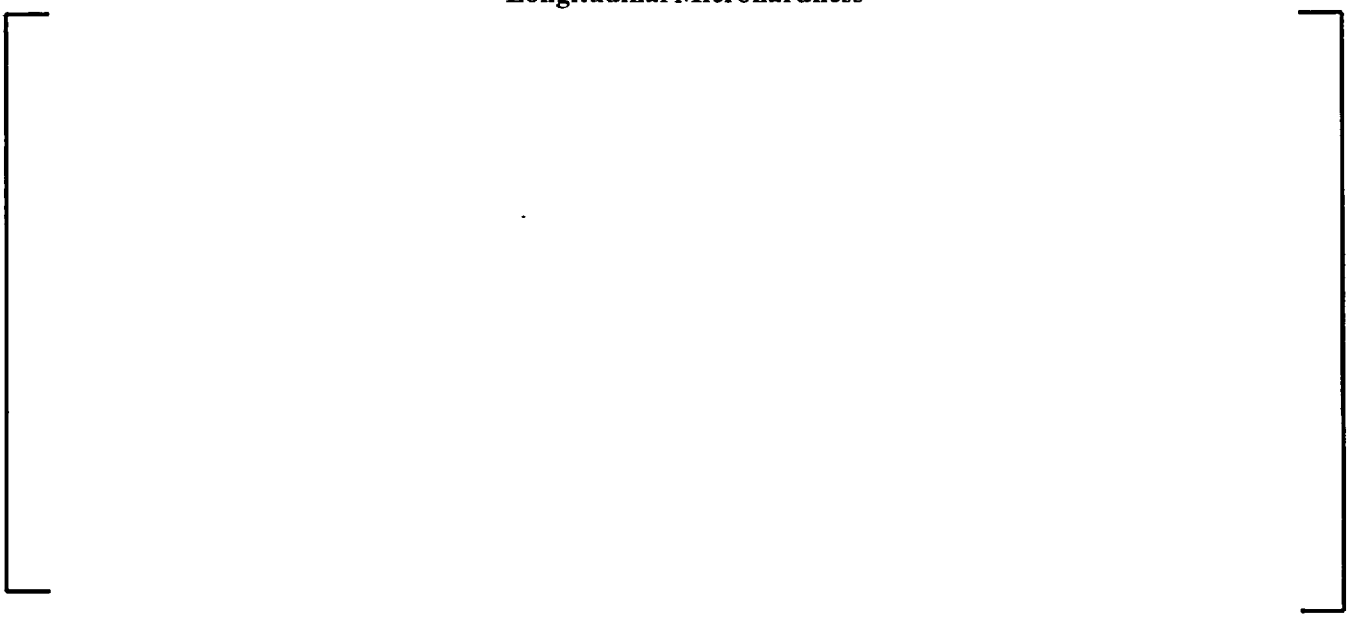

Figure B.8-2
Transverse Microhardness

a, b, c

a, b, c

Table B.8-1
Microhardness Data

[

]

B.9 Creep:

Results: [

]a, b, c

Figure B.9-1
Optimized ZIRLO™ and Standard ZIRLO™ Thermal Creep Data

a, b, c

[

]

B.10 Fatigue:

Results: The fatigue test results and the Westinghouse fatigue design limit are plotted in Figure B.10-1.

Figure B.10-1
Optimized ZIRLO™ Fatigue Test

a, b, c

B.11 Texture:

Results: [

]a, c

Table B.11-1
Optimized and Standard ZIRLO™ Texture Values

a, b, c

a, b, c

[

]

a, b, c

[a, b, c]

[

] a, c

B.12 Corrosion:

Results: [

] a, b, c

Figure B.12-1
800 °F Corrosion Test

a, b, c

[]

Table B.12-1
800 °F Steam Corrosion Test Results

a, b, c

[ ]

Figure B.12-2
680 °F Corrosion Test

[a, b, c]

Table B.12-2

[a. b. c]

B.13 Single Rod Burst Tests

Results: [

] a, b, c

[

]^{a,b,c}. As shown in Figure B.13-1, the new data for Standard and Optimized ZIRLO™ are indistinguishable from the prior ZIRLO™ data.

[

]^{a,b,c}.

a, b, c

Figure B.13-1

[ ]

Figure B.13-2

a, b, c

Table B.13-1
Standard ZIRLO™ Burst Test Control Data for Comparison to Optimized ZIRLO™

a, b, c

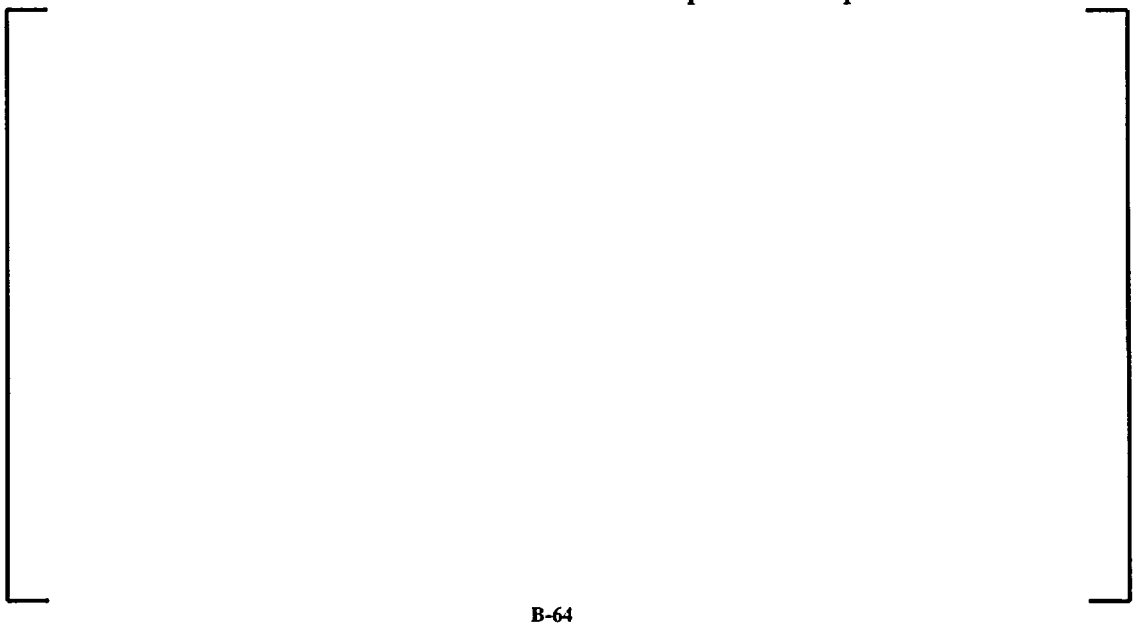

Table B.13-2
Optimized ZIRLO™ Burst Test Data

a, b, c

B.14 High Temperature Creep Test:

Results: [

]$^{a, b, c}$

As shown in Figure B.14-1, the Standard and Optimized ZIRLO™ creep rates are in reasonable agreement with the current ZIRLO™ model for temperatures between [

]$^{a, b, c}$

Figure B.14-1
Creep Rates for Standard and Optimized ZIRLO™

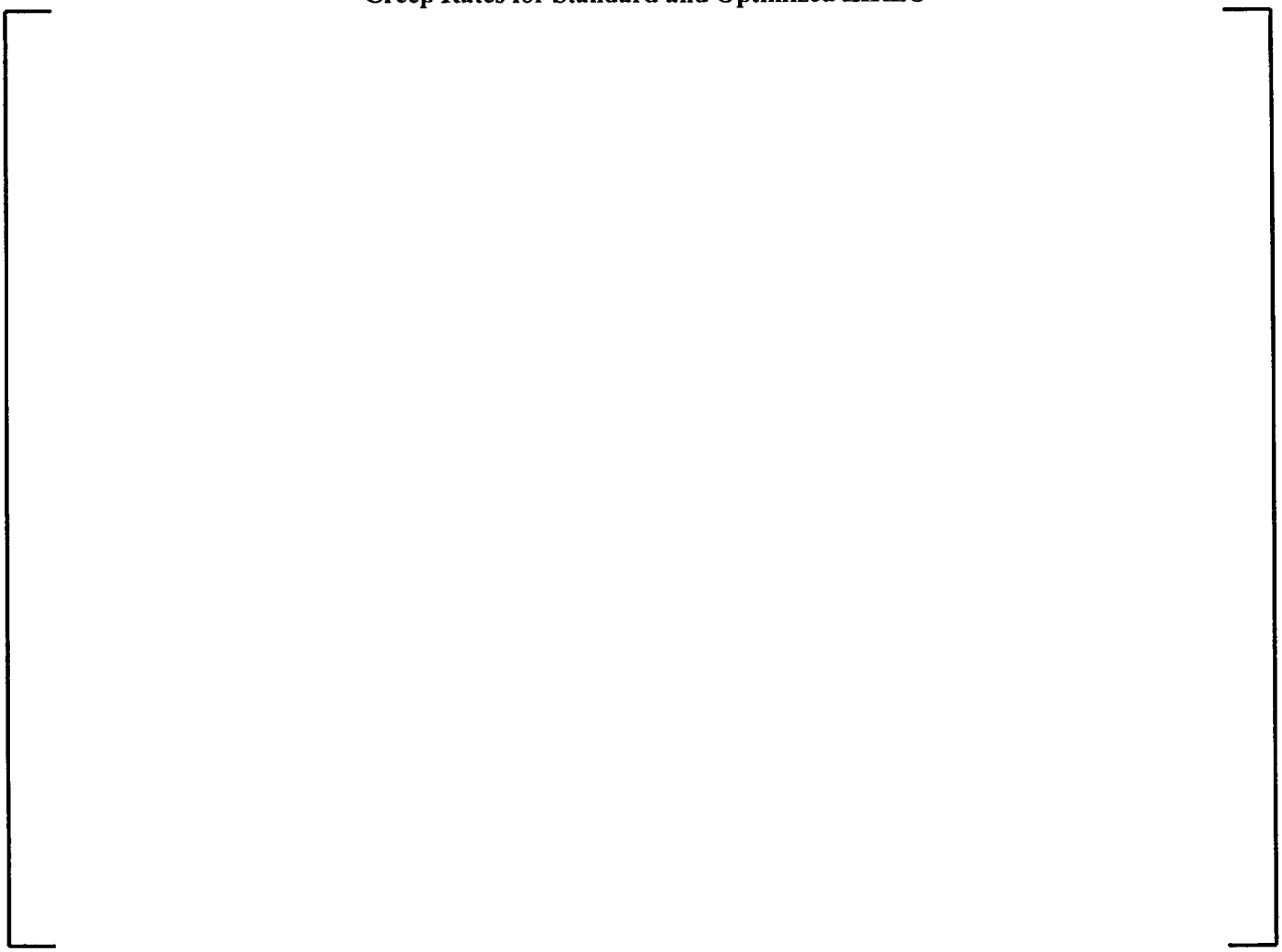

a,b, c

Table B.14-1
Creep Rates for Optimized ZIRLO™

a, b,c

[ ]

Table B.14-2
Creep Rates for Standard ZIRLO™

a, b c

[ ]

B.15 Metal Water Reaction Test:

Results: [

] [a, b, c] All of the test data fall well below the Baker-Just model. This satisfies the 10 CFR 50 Appendix K requirement that Baker-Just be used to conservatively predict the oxidation behavior of the cladding under LOCA conditions. [

] [a, b, c]

The calculated reaction rates are provided in Table B.15-1.

Table B.15-1
Reaction Rates for Standard and Optimized ZIRLO™

[a, b c]

Figure B.15-1
Reaction Rates for Standard and Optimized ZIRLO™

a, b, c

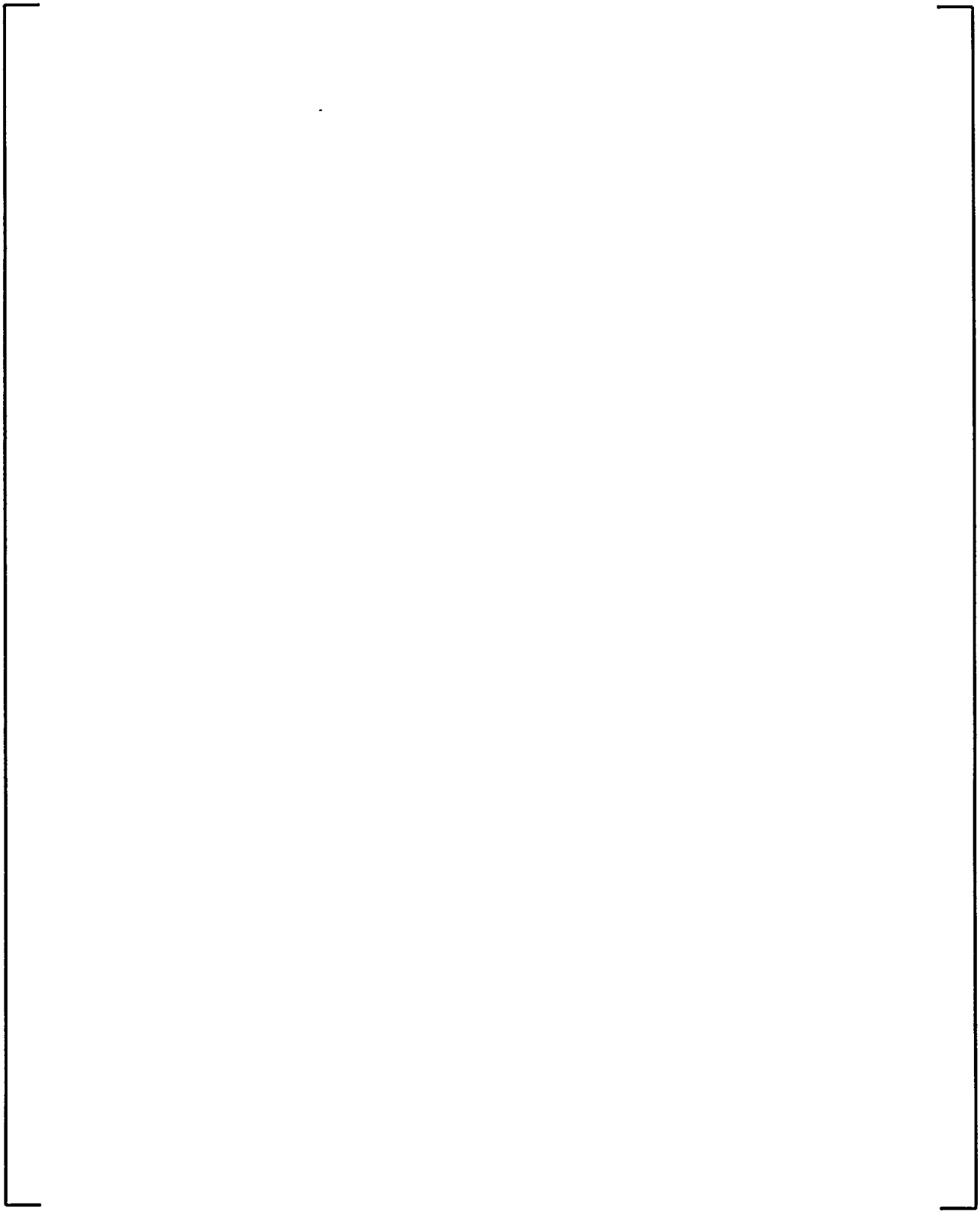

B.16 Ring Compression Test:

Results: The results for the 275°F ring compression tests for two lots of the Optimized ZIRLO™ and for one lot of Standard ZIRLO™, which was the reference case, are shown graphically in Figure B.16-1. [

]^{a,b,c}

[

]^{a,b,c} This data is presented for information only. [

]^{a,b,c}

Based on these tests, all of the 275°F ring compression tests satisfy the 10% relative displacement criterion at ECR values above 17%, satisfying the minimum ductility requirement. The majority of the Standard ZIRLO™ and the Optimized ZIRLO™ data points fall within the population of ZIRLO™ data collected previously and presented to the NRC staff. To summarize, the following conclusions may be drawn from these observations:

- The Optimized ZIRLO™ satisfies the minimum ductility requirement for material oxidized to 17% ECR,
- The retained ductility of the Optimized ZIRLO™ is effectively the same as that of Standard ZIRLO™, [
-

]^{a,b,c}

Figure B.16-1
Relative Displacement versus Equivalent Clad Reacted (ECR) at 275°F

[a, b, c]

Table B.16-1
Ring Compression Test Results

[a, b, c]

Table B.16-2
Ring Compression Test Results for Samples Oxidized at 1300°C

a, b, c

[

]